The Pennsylvania State University

The Graduate School

College of Earth and Mineral Sciences

SIMULATIONS OF AEROSOL, MICROPHYSICAL AND COASTAL INFLUENCES ON ARCTIC MIXED-PHASE CLOUDS

A Dissertation in

Meteorology

by

Alexander Elkov Avramov

Submitted in Partial Fulfillment
of the Requirements
for the Degree of

Doctor of Philosophy

May 2009

The dissertation of Alexander Elkov Avramov was reviewed and approved* by the following:

Jerry Y. Harrington
Associate Professor of Meteorology
Dissertation Advisor
Chair of Committee

Johannes Verlinde
Associate Professor of Meteorology

Eugene E. Clothiaux
Associate Professor of Meteorology

David Pollard
Senior Research Associate

William H. Brune
Professor of Meteorology
Head of the Department of Meteorology

*Signatures are on file in the Graduate School

ABSTRACT

Mixed-phase stratus clouds are the prevalent cloud type in the Arctic during the winter and transition seasons. Despite their important role in various climate feedback mechanisms they are still not well understood and are difficult to represent accurately in large-scale models. In this study the role of ice nucleation mechanisms, the influence of the coastally-generated circulations and parameterized ice crystal habit on the longevity and structure of Arctic mixed-phase clouds were examined using detailed mesoscale, cloud- and eddy-resolving model simulations.

The structure and the lifetime of simulated Arctic mixed-phase clouds were found to be highly sensitive to the concentration of ice-nuclei (IN) acting in deposition/condensation-freezing nucleation mode. Contact nucleation could not produce significant ice amounts unless the contact IN concentrations were increased to unrealistically high values. Local, coastally induced circulations were found to be responsible for maintaining the continuous ice precipitation along the coastline through transport of deposition/condensation-freezing IN from above the cloud layer. It was demonstrated that incorrect partitioning of the liquid and ice phase can produce errors in the surface radiative budget of up to 90 Wm^{-2}.

Simulated IN sensitivity and liquid/ice phase partitioning were found to depend critically on the assumed ice crystal habit. It was demonstrated that a large range of liquid or ice water path can be produced by reasonable changes in

ice crystal habit mass-dimensional and terminal fall-speed relations based on data reported in the literature. The changes in ice crystal habit were shown to be related to liquid layer formation, splitting of liquid layers, and cloud dissipation mechanisms in multi-layered Arctic mixed-phase clouds. These results suggest that predicting changes in crystal habit is of significant importance for correct model representation of mixed-phase clouds.

Three additional ice nucleation mechanisms (“evaporation IN”, “evaporation freezing”, and immersion freezing) were examined regarding the ability of our model to more accurately simulate liquid and ice water content, ice concentrations, and observed cloud structure. All of these mechanisms were found to be capable of producing ice crystal concentrations similar to the observed values, while maintaining the liquid content of the cloud. The observed cloud structure was also correctly reproduced for extended periods of time.

TABLE OF CONTENTS

LIST OF FIGURES

LIST OF TABLES

ACKNOWLEDGEMENTS

First and foremost, I would like to thank my academic advisor and mentor, Dr. Jerry Harrington, without whom I would not have the knowledge and motivation to complete this dissertation. I am indefinitely indebted to the members of my committee, Dr. Johannes Verlinde, Dr. Eugene Clothiaux, and Dr. David Pollard, for the quidance, extreme patience, encouragement and criticism they have provided me with during my time in graduate school.

My officemates, Lindsay Sheridan, Steven Greenberg, Nat Johnson, and Victor Yannuzzi, an interesting group of individuals, who significantly contributed to my graduate school experience, definitely deserve a special mention.

I would also like to acknowledge Maria Herrmann, for being such a good friend and putting up with me, Mahlon Rambukange, for the numerous productive discussions on mixed-phase clouds, and Chad Bahrmann, who always had all the answers. Last, but not in any way least, I would like to thank Linda Porta, who made sure that I met most of the graduate school deadlines.

Chapter 1

Introduction

The polar regions of the Earth have been recognized for a long time as playing a major role in the Earth's climate. Results from global climate model (GCM) simulations indicate that the polar regions are the most sensitive of any region of the Earth to global environmental changes (Houghton et al., 1990). Despite the differences between individual models in response to doubled CO2 concentration in the Earth's atmosphere, nearly all simulations predict temperature changes in Arctic regions that are at least two to three times higher than the global mean change (Houghton et al., 1990). Conversely, it is believed that the Arctic plays a significant role in global climate control, mainly through its influence on the large-scale thermohaline circulation of the oceans and on the global heat budget (Tao et al., 1996).

In a recent GCM study, Vavrus (2004) showed that at least 40% of the annual Arctic warming in a doubled CO2 scenario comes from cloud-climate interactions. Clouds have a two-fold effect on the surface radiation budget – they warm the surface through emission of infrared radiation and at the same time they cool the surface by increasing the shortwave albedo. Long-wave cloud forcing is a function of cloud temperature, height and microphysics, while short-wave forcing depends on those factors along with the surface albedo and the

solar zenith angle (Curry et al., 1996; Shupe and Intrieri, 2004). In mid-latitudes it is widely accepted that low-level clouds generally lead to surface cooling, i.e. the solar albedo effect dominates over the long-wave effect, while the opposite is believed for high-level cirrus clouds. In the Arctic, however, the presence of highly reflective snow/ice surfaces might lead to a reversal of the low-level cloud impact. Using cloud and radiation measurements, taken during the Surface Heat Budget of the Arctic (SHEBA) experiment, Shupe and Intrieri (2004) investigated the cloud radiative forcing of the Arctic surface. They found that clouds exert a radiative warming effect on the surface during most of the year. Over a short period in the middle of the summer, the solar albedo effect surpasses the long-wave effect and cloud presence induces a surface cooling.

In an overview of Arctic cloud and radiation characteristics, Curry et al. (1996) provide a detailed discussion of a variety of feedback mechanisms thought to operate in the Arctic. In addition to the temperature-ice-albedo and water vapor feedbacks, they considered four cloud-radiation feedback mechanisms: cloud fraction feedback, cloud liquid water content feedback, cloud drop size feedback and cloud-temperature feedback. To examine the strength of the different feedback processes locally in the Arctic, they calculated the feedback gain ratio for each of the feedback mechanisms. They noted that the magnitude, and even the sign, of some of the feedback processes are associated with significant uncertainties. Furthermore, because the individual feedback mechanisms are intrinsically linked to each other, it is not possible to determine their individual contribution to the total feedback and rank them. Nevertheless,

their results illustrate the importance of Arctic cloud processes to the Arctic climate and the global climate system.

Mixed-phase stratus clouds are the prevalent cloud type in the Arctic during the winter and transition seasons (roughly mid-August through mid-June). Due to the Bergeron process, mixed-phase clouds are usually thought to be short-lived: because of the difference of saturation vapor pressure over ice and liquid water, the ice crystals in a mixed-phased cloud will grow at the expense of the cloud droplets. Subsequent precipitation of the ice may then cause the complete glaciation of the cloud. However, the liquid phase is commonly found in Arctic stratus clouds (Pinto, 1998; Hobbs and Rangno, 1998; Shupe et al. 2006; Prenni et al., 2007) at subfreezing temperatures. Hobbs and Rangno (1998) observed persistent liquid-water cloud tops at temperatures as low as -31 °C. In the Arctic mixed-phase cloud systems are quite persistent – lasting from a few days to over a couple of weeks. Because of their longevity and the presence of the radiatively-important liquid phase they can strongly affect the surface energy budget (Shupe and Intrieri, 2004; Zuidema et al., 2005) and consequently the freezing and melting rate of the Arctic ice pack (Jiang et al., 2000). The persistence of mixed-phase clouds is one of the major challenges for any model.

The ability of the current regional and global climate models to correctly simulate mixed-phase clouds was explored as part of the Arctic Climate Model Intercomparison Project (Curry and Lynch, 2002). During the summer all of the models predicted liquid water paths similar to the observed values; however,

during the winter all of the models produced very little or no liquid water at all (Prenni et al., 2007).

At present, how mixed-phase Arctic clouds can maintain significant quantities of supercooled liquid water and ice for extended periods of times and at very low temperatures, is not completely understood. Several hypotheses have been suggested in an effort to explain mixed-phase cloud persistence. Rauber and Tokay (1991) found that if the ice crystals at the top of the cloud are small, the imbalance between the condensate supply rate (dynamic forcing) and the bulk ice crystal mass growth is enough to produce and maintain a cloud-top supercooled liquid layer. If dynamic forcing produces parcel oscillations with sufficiently strong vertical motion, both liquid and ice can be maintained for extended periods of time (Korolev and Isaac, 2003; Korolev and Field, 2008). Pinto (1998) and Harrington et al. (1999) hypothesized that mixed-phase clouds are maintained through a balance between liquid water condensation resulting from the cloud-top radiative cooling and ice removal by precipitation. In their modeling studies Harrington et al. (1999) and Harrington and Olsson (2001a) found that this balance depends strongly on the ambient concentration of deposition ice nuclei (IN) and possibly on the crystal habit assumed (which controls vapor uptake and sedimentation rates). While the Harrington et al. (1999) study used a detailed, bin microphysical model, a follow-on study by Jiang et al. (2000) showed that similar results could be obtained with a simpler, bulk microphysical scheme.

All of the modeling studies in the preceding paragraph require low ice concentrations (through low IN concentrations) to maintain supercooled liquid water. Many recent and older measurements of IN concentrations in the Arctic support this notion (Bigg, 1996; Rogers, 2001; Prenni et al., 2007) with most measurements showing IN concentrations of $< 1\ L^{-1}$ with some large excursions. However, unresolved questions remain with respect to how ice is initiated in Arctic mixed-phase clouds and ice clouds in general.

Morrison and Pinto (2005) implemented a new dual-moment bulk microphysics scheme into the polar version of MM5 in a mesoscale modeling study of mixed-phase stratus clouds observed during SHEBA. In contrast to the previous studies of Harrington et al. (1999), Harrington and Olsson (2001a) and Jiang et al. (2000), they found that the primary ice nucleation mode in their simulations is contact freezing of cloud droplets. Using a 1-D cloud model and a different treatment of ice nucleation Morrison et al. (2005) found that the liquid phase is highly sensitive to the number concentration of deposition/condensation-freezing nuclei and much less sensitive to the number of contact nuclei. They subsequently developed a conceptual model of Arctic mixed-phase clouds that explains cloud persistence through the rapid depletion of deposition/condensation-freezing nuclei and a self-regulating negative feedback involving drop freezing by contact nucleation. In contradistinction, Avramov and Harrington (2006) could not produce significant ice water amounts by contact nucleation in their mesoscale simulations unless the contact IN concentrations were assumed to be as high as that reported by Young (1974),

which are considered to be too large (e.g., Meyers et al., 1992). It is important to note that the case simulated by Avramov and Harrington (2006) was at least 3-6 degrees warmer, with a larger liquid water path, than the case simulated by Morrison et al. (2005).

In recent simulations of the Mixed-Phase Arctic Cloud Experiment (M-PACE) (Verlinde et al., 2007) case, Prenni et al. (2007) were able to maintain mixed-phase stratus only if the IN concentration were as low as the observed values, and if deposition/condensation-freezing IN are removed through precipitation, following Harrington and Olsson (2001a). Furthermore, this observed case occurred during on-shore flow along the northern Alaska coast. Avramov and Harrington (2006) suggested that mesoscale circulations, generated along the coastline, continued to bring IN-rich air into the boundary layer along the coast. This produced a continual band of precipitation along the coastline, similar to what was observed. Regardless, Avramov and Harrington's (2006) and Prenni et al.'s (2007) simulations produce too little ice water content and ice concentration, and no precipitation bursts such as those observed. The primary nucleation mechanism in Avramov and Harrington's (2006) and Prenni et al.'s (2007) simulations were deposition/condensation-freezing.

In a later study, Morrison et al. (2008a) investigated the sensitivity of mixed-phase stratocumulus to cloud condensation and ice nuclei during the M-PACE. Their results are consistent with the previous work of Harrington et al. (1999) although reported sensitivities to IN concentrations are somewhat lower

than those previously reported. Also, some uncertainties with respect to the IN-depleting mechanism still remain.

The uncertainties in ice nucleation mechanism are connected intimately to the underlying cloud dynamics. Variations in ice nucleation alter ice concentrations, affecting both ice crystal vapor uptake through changes in crystal surface area and ice crystal sedimentation rates. Both of these processes can then influence the dynamics of mixed-phase clouds. For instance, the eddy resolving model (ERM) simulations of Harrington et al. (1999) showed that mixed-phase clouds can support enhanced ice crystal concentrations as long as the latent heating due to ice growth does not overpower the cloud top radiative cooling which drives the buoyant eddies. Furthermore, Harrington and Olsson (2001a) showed that even strongly surface-driven mixed-phase clouds are dynamically influenced by ice precipitation: Ice precipitation tends to stabilize downdrafts leading to a reduction in turbulent kinetic energy throughout the boundary layer. It is important to note that these works considered ice concentrations produced by nucleation mechanisms that are spread spatially throughout the cloud deck. Hence, these studies apply mainly to cases where ice exists everywhere throughout the liquid portion of the cloud.

Some of the measurements cited above suggest that mixed-phase clouds contain small pockets of high ice concentrations embedded within the liquid and the simulations just cited cannot reproduce this observation. However, recent Large Eddy Simulation (LES) studies of the M-PACE case by Fridlind et al. (2007) have included nucleation mechanisms that are postulated to occur on a

smaller spatial scale. As has been shown in prior papers, deposition IN nucleate and are rapidly removed from the cloud layer through precipitation in their simulations. The only way that Fridlind et al. (2007) can maintain liquid while obtaining realistic ice concentrations, and ice water content bursts, is through either the proposed “evaporation nucleation” mechanism (Cotton and Field, 2002) or “evaporation IN” (Rosinski and Morgan, 1991) . During drop evaporation (Cotton and Field, 2002), it is hypothesized that a fraction of the evaporating drops freeze. A second hypothesis is that during evaporation, IN are released (Rosinski and Morgan, 1991). While these proposed mechanisms are not new, it is the first time that they have been used in a modeling study of mixed-phase Arctic clouds. Though no physical explanation exists for either of these mechanisms, they could at least ostensibly explain the pockets of high ice concentrations that are sometimes found in these clouds (e.g. Hobbs and Rangno, 1998). Moreover, Fridlind et al. (2007) show that none of the other proposed mechanisms can produce liquid and ice profiles that consistently match observations.

While all prior studies focus, primarily, on ice nucleation and ice concentrations, it is also true that ice habit and how it is parameterized affects the microphysical structure of mixed-phase Arctic stratus. Liquid water evaporation by ice crystals depends not only on their concentration but also on their in-cloud residence time and their mass growth rate. The in-cloud residence time depends on the sedimentation velocity of the crystals, which is controlled by their habit and size. The mass growth rate depends on the shape of the crystals

and size, which in turn depends on the ice concentration. Hence, the phase-partitioning within mixed-phase stratus may depend significantly on how the habit of the crystals is parameterized. Consequently, one might expect that a cloud's sensitivity to IN concentration would vary depending on the assumed ice crystals shape. Indeed, in a simplified example, Harrington et al. (1999) showed that changing ice habit from plates to spheres may have a substantial effect on mixed-phase cloud evolution. Moreover, many models use different parameterizations for crystal habit, which may lead to substantial differences in the final model results.

In the light of results of the previous studies we suggest that the following topics need further exploration and will be examined in this dissertation:

(1) All microphysical parameterizations are forced to use simplified formulations for crystal habit that are uncertain. What is the influence of the assumed ice crystals habit on IN sensitivities, cloud dynamics, and cloud lifetime?

(2) During M-PACE, multi-layered clouds were observed over a three day period. What are the microphysical and aerosol influences (IN concentration, ice crystals habit, fall speeds) on multi-layered cloud formation and evolution?

(3) The M-PACE study occurred along the northern Alaskan coast and it is well known that coastal regions induce mesoscale circulations that affect coastal cloudiness. What is the role of these coastally-generated circulations in transporting IN both vertically and horizontally? How are clouds subsequently affected?

(4) What is the relative importance of the different heterogeneous ice nucleation modes in producing the structure of mixed-phase clouds, including the evaporation nuclei hypothesis put forward by Fridlind et al. (2007) ?

To explore these areas we will use eddy-resolving, cloud-resolving and high resolution meso-scale modeling to simulate mixed-phase Arctic clouds observed during the recent Mixed-Phase Arctic Cloud Experiment. We will focus on two periods: 9-11 October, when single layer mixed-phase clouds were observed, and 5-8 October, when several liquid layers were present with ice crystals settling between them.

Chapter 2

Model description

The model used in this study is the Colorado State University version of the Regional Atmospheric Modeling System (RAMS@CSU; Cotton et al., 2003) with two-moment bulk microphysics (Walko et al., 1995; Meyers at al., 1997) and a two-stream radiation scheme (Harrington, 1997; Harrington and Olsson, 2001b). RAMS is a nested-grid model which allows for the simulation of large-scale features (up to global) with nested grids that allow for fine resolution down to the scale of individual clouds. In simulations presented in the following chapters the model was used in three different configurations: three-dimensional nested grid meso-scale model (Chapter 3), two-dimensional cloud resolving model (Chapter 4) and two-dimensional eddy-resolving model (Chapter 5).

The latest version of RAMS has many components that make it appropriate for Arctic cloud simulations. It has detailed sea-ice and soil-vegetation surface models suitable for the Arctic (Cotton et al., 2003). The availability of the sea-ice model is important, as it regulates surface heat and moisture fluxes which strongly influence cloud processes. The microphysical package has seven hydrometeor categories: cloud droplets, rain, pristine ice, snow, aggregates, graupel and hail. The number density of hydrometeors in each category is described using the complete gamma distribution function (Walko et al. 1995) as:

$$n(D) = \frac{N_t}{\Gamma(\nu)} \left(\frac{D}{D_n} \right)^{\nu-1} \frac{1}{D_n} \exp\left(-\frac{D}{D_n} \right), \tag{2.1}$$

where N_t is the number concentration of hydrometeors of given type, ν is the distribution shape parameter (different for each category), $\Gamma(\nu)$ is the gamma function of ν, D is the hydrometeors size, and D_n is the characteristic diameter of the distribution which serves as a diameter scaling factor for the distribution. Two moments of the distribution, the total mixing ratio and number concentration, are explicitly prognosed in the model for each of the categories. In our simulations only the mixing ratio is predicted for cloud droplets. Pristine ice, snow and aggregates are assumed to be completely frozen, while graupel and hail are allowed to have a liquid fraction.

Pristine ice and snow categories are primarily vapor grown and so allow for a bi-modal ice crystal distribution in the model (Figure 2.1). The pristine ice category represents relatively small crystals (mean size $\equiv \overline{L} < 125\ \mu\text{m}$), into which ice nucleates from vapor. Once formed, pristine ice crystals grow by vapor deposition and a small amount of riming. Snow is defined as larger ice crystals ($125\,\mu\text{m} < \overline{L} < 10\,\text{mm}$) which grow by vapor deposition and a moderate amount of riming. The snow category is initiated by a transfer of number concentration and mixing ratio from the pristine ice category by vapor deposition. At sub-saturated conditions the converse transfer is carried out from snow to pristine ice and from pristine ice to vapor (Harrington et al., 1995).

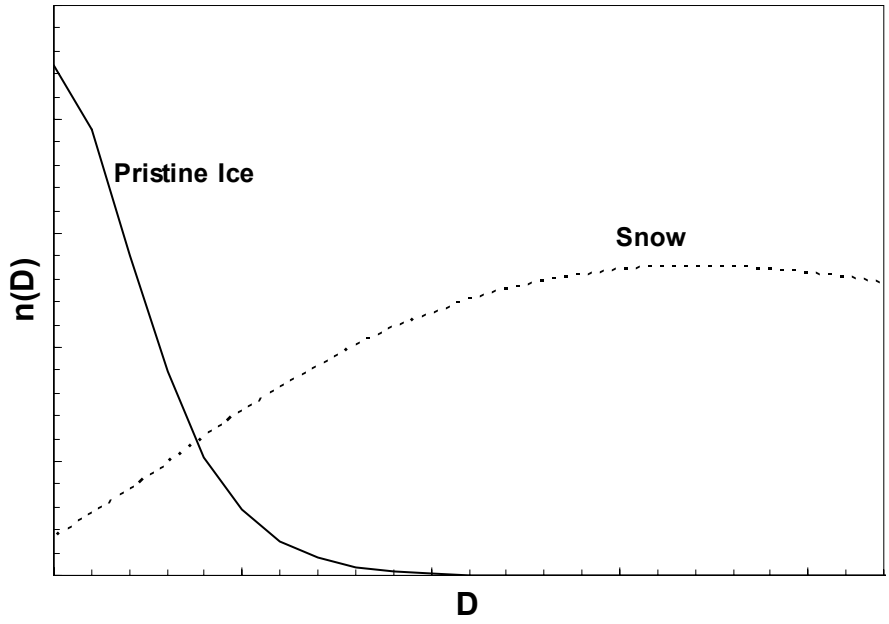

Figure 2.1: Schematic representation of the bi-modal ice distribution. The pristine ice distribution (solid line) has a shape factor of $\nu = 4$ and snow (broken line) has a shape factor of $\nu = 3$

Aggregates form by collection events between pristine ice, snow and aggregates. Graupel is assumed to be a spherical, intermediate density hydrometeor formed by riming or partial melting of pristine ice, snow and aggregates. It is allowed to carry only a small liquid fraction. If the amount of liquid becomes larger, graupel particles are transferred into the hail category. Hail is a high density hydrometeor, formed by riming or partial melting of graupel or freezing of rain drops. It is allowed to carry any fraction of liquid water.

Pristine ice crystals are nucleated through heterogeneous nucleation, which requires the presence of IN, and homogeneous freezing of supercooled cloud droplets. The homogeneous freezing in the model is parameterized following DeMott et al. (1994) and is applied at temperatures lower than -30°C.

Three of the four heterogeneous nucleation modes (Figure 2.2) are explicitly parameterized in the model: condensation-freezing, deposition and contact freezing (Meyers et al., 1992).

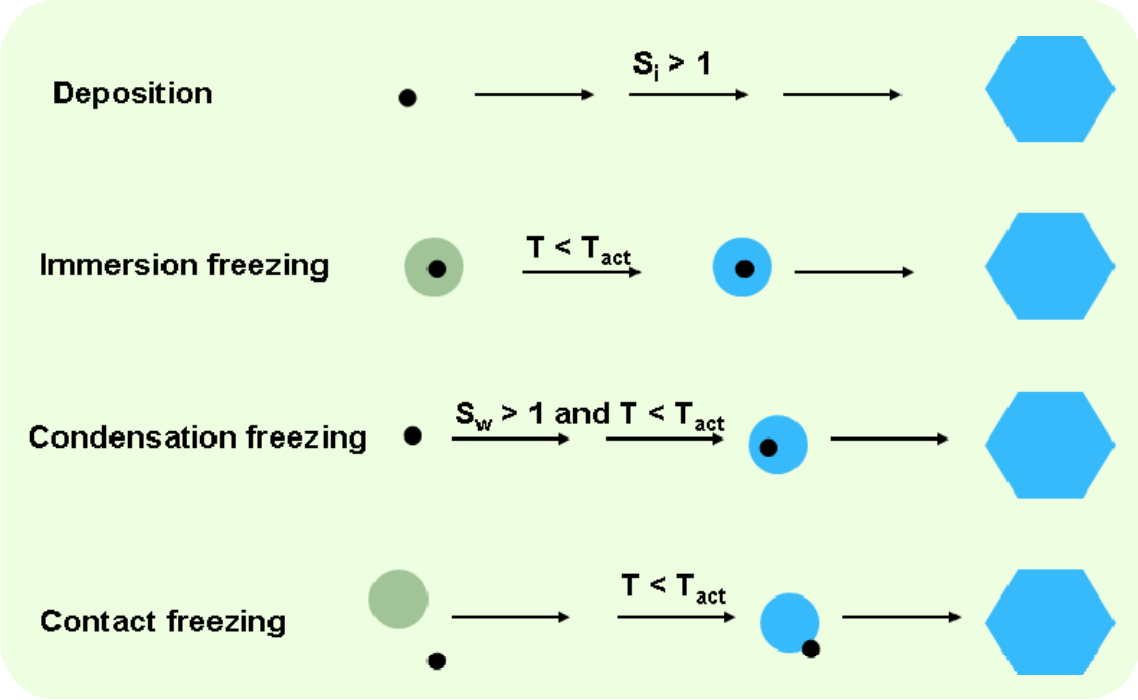

Figure 2.2: Schematic representation of the basic nucleation modes

Condensation-freezing nucleation occurs when an aerosol is capable of acting as a cloud condensation nucleus (CCN) and an IN simultaneously. The aerosol particle acts as a CCN initially to form a cloud drop which then freezes forming an ice crystal. In the deposition nucleation mode vapor molecules produce ice as they attach to the IN. The number of IN acting in deposition and condensation-freezing modes is parameterized as a single function of ice supersaturation, following Meyers et al. (1992):

$$N_d = \exp(a + bS_i), \tag{2.2}$$

where N_d is the number of nucleated crystals (L^{-1}), S_i is the ice supersaturation and *a* and *b* are empirically-derived coefficients. Prenni et al. (2007) showed that the Meyers parameterization, which is based on mid-latitude observations, significantly overestimates IN concentration for Arctic regions. Using IN data collected during M-PACE, Prenni et al. (2007) determined values for coefficients *a* and *b* (*a* = -1.488, *b* = 0.0187) that better approximate Arctic values. For the conditions encountered during M-PACE the new parameterization predicts IN concentrations of ~ 0.15 L^{-1}, a factor of 26 lower than the Meyers parameterization.

Contact freezing nucleation occurs when an IN comes in contact with a supercooled cloud droplet. The IN is transported to the surface of the droplet by a combination of diffusiophoresis, thermophoresis and Brownian motion, though Brownian motion dominates. Pristine ice production by contact nucleation is parameterized following Cotton et al. (1986) :

$$\left(\frac{dN}{dt}\right)_c = N_a(F_B + F_d + F_t), \tag{2.3}$$

where N_a is the number of IN available for contact nucleation and F_B, F_d and F_t terms represent the Brownian motion, diffusiophoresis and thermophoresis processes respectively. Parameterization of these terms is discussed in detail in Cotton et al. (1986). N_a is parameterized as a function of temperature, as described in Meyers et al.(1992):

$$N_a = \exp\left(a + b(273.15 - T_c)\right), \tag{2.4}$$

where N_a is the number of contact IN (L^{-1}), $a = -2.80$, $b = 0.262$ and T_c is the cloud droplet temperature. The coefficients in the above formula were empirically-derived from mid-latitude data. Since there are no available contact IN observational data from the Arctic, we assume (somewhat arbitrarily) that contact IN concentration should scale with the deposition/condensation-freezing IN concentration and so we reduced contact IN by a factor of 26.

In addition to these ice nucleation modes, in simulations presented in Chapter 5 we included another three ice production mechanisms: immersion freezing, evaporation freezing and releasing of IN during droplet evaporation. Immersion freezing occurs when an IN is already immersed in a supercooled cloud droplet. Freezing is initiated when the temperature of the droplet becomes sufficiently low (Figure 2.2). According to Bigg (1953), the nucleation rate due to immersion freezing depends on the number of drops, their mass and the amount of supercooling:

$$\frac{dN_{if}(m,t)}{dt} = N_w(m,t)\frac{m}{\rho_w}\overline{A}.\exp\left[\overline{B}\left(T_0 - T\right)\right], \tag{2.5}$$

where N_{if} is the number of frozen drops with mass m and $\overline{A}$ and $\overline{B}$ are empirically derived parameters having values of 10^{-4} cm^{-3} s^{-1} and 0.66 deg^{-1}, respectively.

Parameterization of ice nucleation on IN released during droplet evaporation ("evaporation IN") is based on Rosinski and Morgan (1991) findings.

In their cloud chamber experiments they observed IN formation from residuals of a small fraction of evaporating cloud droplets. According to Rosinski and Morgan (1991), the high concentration of cloud droplets and the positive feedback involved can accelerate this process, so that significant ice crystal concentrations are produced (Figure 2.3). The IN formed by evaporating droplets are found to act in condensation-freezing and/or deposition nucleation modes. The fraction of evaporated droplets that produce IN is estimated to be between 10^{-5} and 10^{-4} (Rosinski and Morgan, 1991).

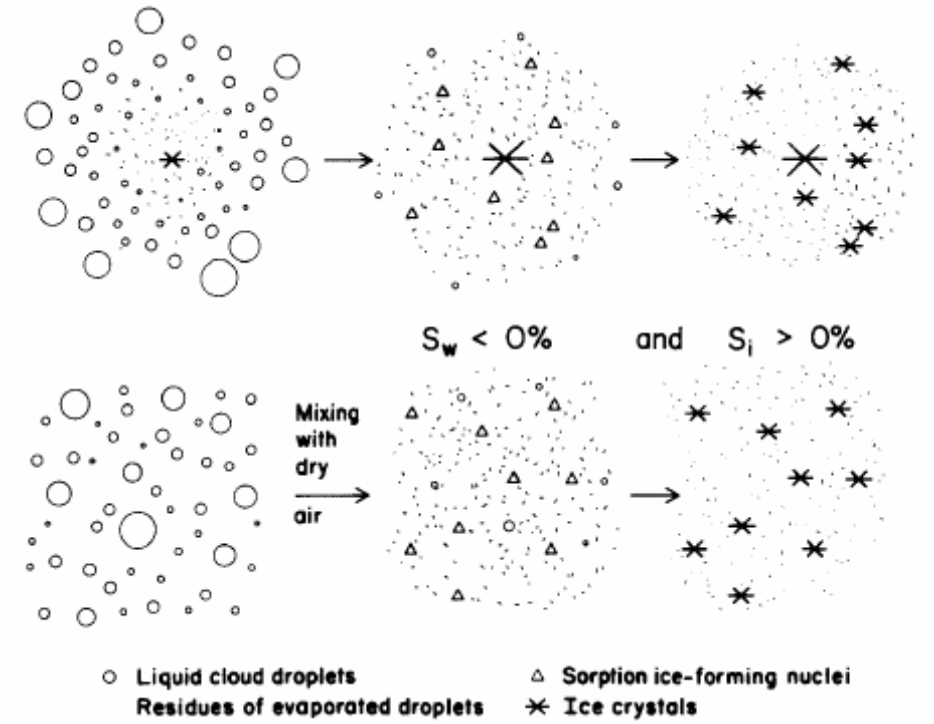

Figure 2.3: Mechanism of ice crystal formation through "evaporation IN" (from Rosinski and Morgan, 1991)

In the "evaporation freezing" hypothesis of Cotton and Field (2002) it is assumed that some fraction of cloud droplets freezes during evaporation,

producing ice crystals. As Cotton and Field (2002) point out, however, this nucleation scheme is not based on any physical mechanism. Instead, it is merely a method of generating observed ice crystal concentrations in model simulations. Consequently, the choice of the freezing rate is not critical. Similar to Fridlind et al. (2007), a trial and error procedure is used to find a freezing rate that produces results close to observations.

In practice, there are two differing interpretations of the deposition/condensation freezing IN measurements that lead to different IN treatment in models. One treatment is termed “diagnostic” and the other is termed “prognostic”. In the diagnostic interpretation, the IN measurements are considered to represent the maximum ice crystal concentration that exists at a given ice super-saturation at all times. The second interpretation considers these measurements as a proxy for the number of IN activated at a given ice supersaturation. Although these interpretations might seem almost identical, their implementation in models is quite different and often produces vastly different results.

In the “diagnostic” approach, the IN parameterization is used in a static fashion: at each time-step the IN concentration is computed with Eq. 2.2 and if the result is greater than the current ice crystal concentration, the difference is nucleated increasing the ice crystal concentration. Hence, throughout the model integration the ice crystal concentration remains at or it is very close to the value predicted by the IN parameterization. In the “prognostic” approach (Harrington and Olsson, 2001a) Eq. 2.2 is evaluated against the number of IN already

activated. Activated IN are removed from the IN population and additional ice nucleation is possible only through supersaturation increase or IN advection from another location. This method mimics IN removal from the atmosphere through crystal growth and subsequent precipitation.

Both “diagnostic” and “prognostic” approaches have their advantages and disadvantages. The “diagnostic” approach is simpler and produces ice concentrations closer to the observed values. On the other hand, the process assumes a constant IN source, which is probably not correct. The “prognostic” approach is more complicated since the model has to keep track of depleted IN mixing ratio in each gridbox and advect it. However, in addition to the option to specify in-situ IN sources, it does provide a means of evaluating the influence of local circulations in transporting IN and/or efficiency of new ice nucleation mechanisms.

We have modified the code so that during a simulation, the model keeps track of the number of IN for both contact and condensation-freezing nucleation modes. The IN concentration is advected by the wind, diffused by turbulence, and depleted when ice crystals nucleate and precipitate out of the atmosphere. The depletion mechanism keeps track of the nucleated aerosol so that these IN are not nucleated in the future. For example, once the initial number of IN in a given model grid-box is depleted, subsequent ice crystal nucleation is possible only if more IN are advected into this grid-box or the supersaturation increases so that more IN are activated. In this study we have adopted the “prognostic” approach for both condensation-freezing/deposition and contact freezing

nucleation mechanisms as we believe that it allows for a more realistic IN treatment in model simulations.

The habits of the ice crystals and how they are parameterized are important for mixed-phase cloud evolution, as we discuss below. The two parameterizations that most strongly affect the water uptake by ice crystals are the mass growth rate and the fall speed, both of which depend on habit. The terminal fall velocity of ice crystals is parameterized following Mitchell (1996):

$$v_t = \alpha_{vt} D^{\beta_{vt}} \ , \tag{2.6}$$

where D is the crystal maximum dimension and α_{vt} and β_{vt} are empirically-derived constants, which differ for each crystal habit. The depositional mass growth rate for a single crystal is given by Walko et al. (1995) as

$$\frac{dm}{dt} = 2\pi D \psi f_{\mathrm{Re}} \left(\rho_{va} - \rho_{vsh} \right), \tag{2.7}$$

where ψ is the vapor diffusivity, m is crystall mass, ρ_{va} is the ambient vapor density, ρ_{vsh} is the equilibrium vapor density over ice, and f_{Re} is the modified ventilation coefficient (Cotton et al., 1982)

$$f_{\mathrm{Re}} = \left[1 + 0.229 \left(\frac{v_t D}{V_k} \right)^{1/2} \right] S \, . \tag{2.8}$$

This formulation includes the shape parameter $S = C/D$, where *C* is the crystal capacitance, and V_k is the kinematic viscosity of the air. Typically, the shape (S) is fixed during a simulation despite the fact that it should change in time (e.g. Chen and Lamb, 1994).

Prognosis of the mass and size requires a functional relationship between the two. Most models use a mass-dimensional relationship like that given by Mitchell (1996):

$$m = \alpha_m D^{\beta_m}, \tag{2.9}$$

where α_m and β_m are empirically-derived constants for each crystal habit. As a consequence of the mass-dimensional relationship and crystal capacitance, different crystal shapes have different growth characteristics. For instance, dendrites grow faster than hexagonal plates because of the greater capacitance, extreme aspect ratio, and larger size of the dendritic crystals (Chen and Lamb, 1994). Physically, this more rapid growth is due to the fact that dendrites have stronger vapor gradients at the tips of the arms.

Chapter 3

Mesosscale simulations of ice nucleation and coastal influences on mixed-phase clouds

Arctic mixed-phase clouds represent a unique challenge for any model. The ability of the current regional and global climate models to correctly simulate these clouds was explored as part of the Arctic Climate Model Intercomparison Project (ARCMIP) (Curry and Lynch, 2002). Figure 3.1 shows some results from this study, in which six regional models are compared to observations from the Surface Heat Budget of the Arctic Ocean (SHEBA) experiment (Uttal et al., 2002). During the summer, all of the models predict liquid water paths similar to

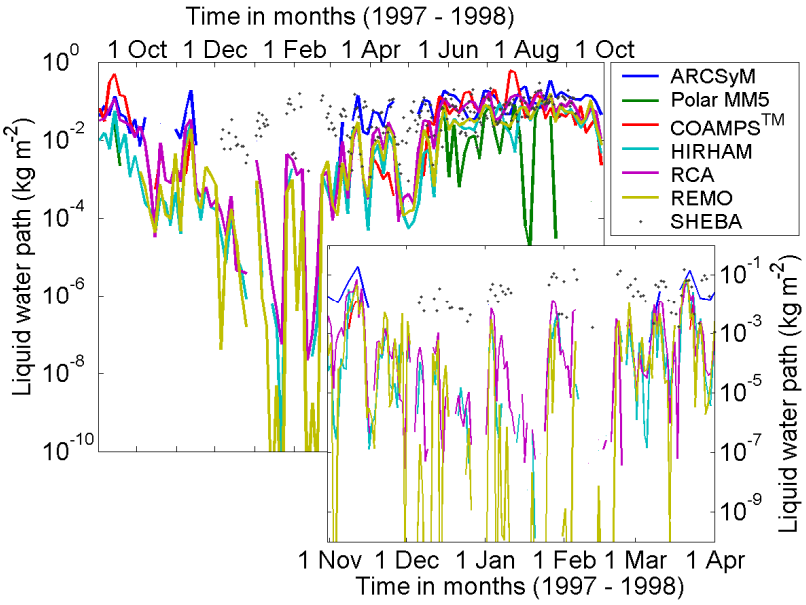

Figure 3.1: Time series of liquid water path (kg m^{-2}) for the SHEBA year. Solid lines are from the six ARCMIP model integrations (see the legend) while black dots are measured by a microwave radiometer at the SHEBA site. Upper panel shows weekly averaged model values for the whole year, while the lower panel shows diurnal averages for winter; SHEBA data are diurnal averages. (From Prenni et al., 2007)

those observed. During winter, however, in contrast to observations, all six models predict very little or no liquid water at all. Results from previous studies of Arctic mixed-phase clouds (e.g. Harrington et al., 1999; Harrington and Olsson, 2001; Jiang et al., 2000) suggest that a possible reason for this discrepancy might be inadequate parameterization of ice nucleation processes. All of these studies required low IN concentrations to maintain supercooled liquid water in simulated clouds. The IN measurements taken during M-PACE (Prenni et al., 2007) tend to support this hypothesis, indicating IN concentrations significantly lower than those used in many models.

Most of the prior studies of Arctic mixed-phase clouds, including those just cited above, used cloud- or eddy resolving models. In fact, the only mesoscale simulation of Arctic mixed-phase clouds known to us is that of Morrison and Pinto (2005). It is therefore interesting to examine the sensitivity of simulated clouds to ambient IN concentrations in a detailed mesoscale model, which allows for mesoscale feedback effects. In this chapter we investigate the influence of ice nucleation mode on the mesoscale structure of Arctic mixed-phase clouds. We examine the roles of both deposition/condensation-freezing and contact nucleation mechanisms and the impact of IN transport by the coastally generated circulations.

3.1 Model configuration

For the simulations in this chapter the model is configured as a three-dimensional meso-scale model with three nested grids (Figure 3.2):

- grid #1 has 64 km horizontal grid spacing; covers the entire state of Alaska – 3392 km x 2368 km;
- grid #2 has a horizontal grid spacing of 16 km and is centered on the North Slope of Alaska,covering a 1296 km x 976 km area;
- grid #3 has 4 km horizontal grid spacing, centered on the north shore (M-PACE domain) and covers area of 312 km x 212 km.

In the vertical, the model has 35 levels and the domain extends up to 15 km height; the vertical grid spacing on all three grids starts with 50 m at the surface and stretches to 1000 m at about 8 km height.

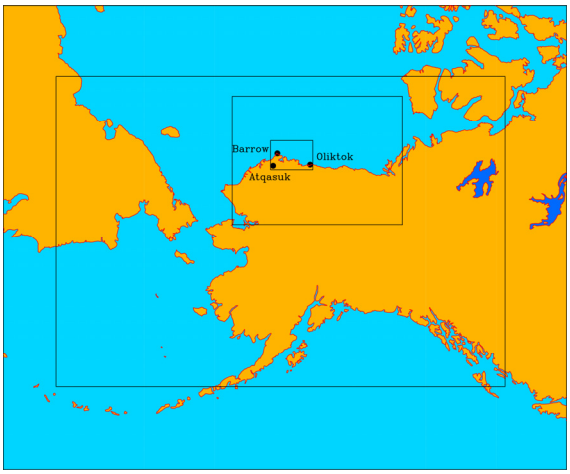

Figure 3.2: Map of the computational domain, showing the three computational grids

The model is initialized using the analyses from the National Center for Environmental Prediction's meso-ETA model grid over Alaska. The sea-ice scheme is initialized with the daily DMSP SSM/I ice dataset and the ocean temperatures are initialized using the NCEP OI SST weekly data. In addition, the outer RAMS grid was nudged to the ETA 12-hourly analyses. As was discussed

in Chapter 2, in these simulations we adopted the “prognosed IN” approach, accounting for IN depletion through precipitation.

3.2 Case description

We simulated the time period of 9-11 October from M-PACE, during which period the North Slope of Alaska and the adjacent Arctic ocean were covered by extensive mixed-phase clouds. The synoptic situation during the simulation period was determined mainly by the high pressure center developing over sea-

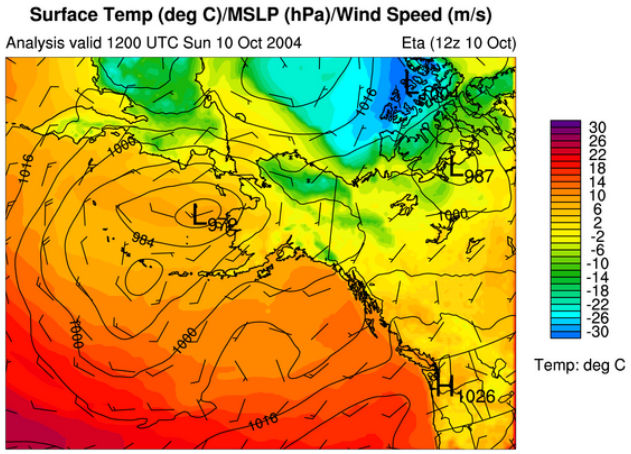

Figure 3.3: ETA surface analysis for 12 UTC October 10, 2004

ice to the north east of the Alaska coast. This high, coupled with the surface low over the Aleutians, intensified the pressure gradient over the area and created favorable conditions for strong easterly winds moving cold air off the pack ice over the relatively warm ocean surface (Figure 3.3). This produced vigorous roll convection and persistent low-level clouds under a sharp inversion that were advected over the NSA (Figure 3.4). No mid- or upper-level clouds were present

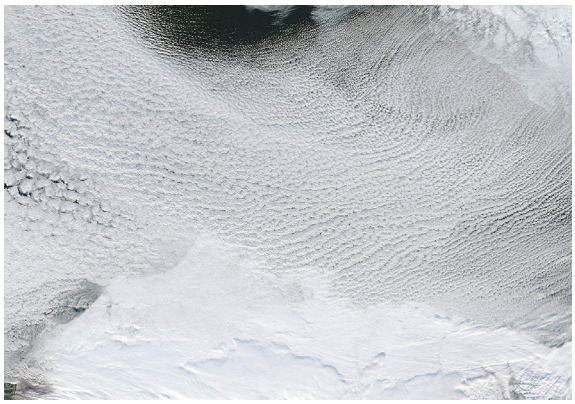

Figure 3.4: MODIS visible image of the North Slope of Alaska on October 10, 2004

during this period. Radar and lidar observations (Figure 3.5) indicate a liquid cloud deck above 800 m elevation with ice precipitation shafts falling from the liquid cloud deck. Representative cloud top temperatures were approximately -17 °C (Verlinde et al., 2007).

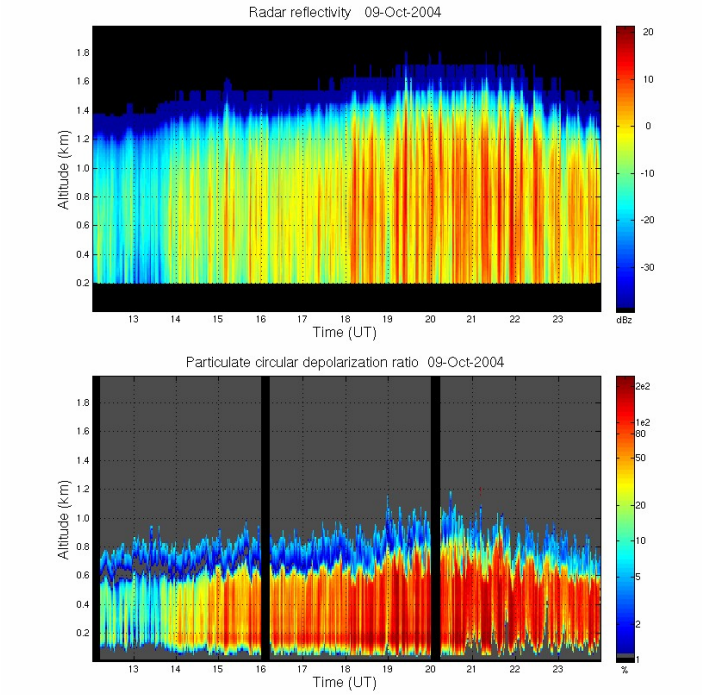

Figure 3.5: MMCR radar reflectivity and HSRL depolarization ratio (<2 liquid, >2 ice) over Barrow, AK

3.3 Results

We first ran a control, or "base", simulation followed by a number of sensitivity tests to examine the impact of IN concentrations and nucleation mode on the life-time of the simulated mixed-phase cloud. Our "base" simulation uses the Meyers et al. (1992) parameterizations for both deposition-condensation-freezing IN and IN available for contact nucleation. Results from the "base" (Standard IN) run are shown on Figure 3.6. After the initial spin-up, the relatively high IN concentrations lead to a rapid conversion of the liquid phase to ice, most

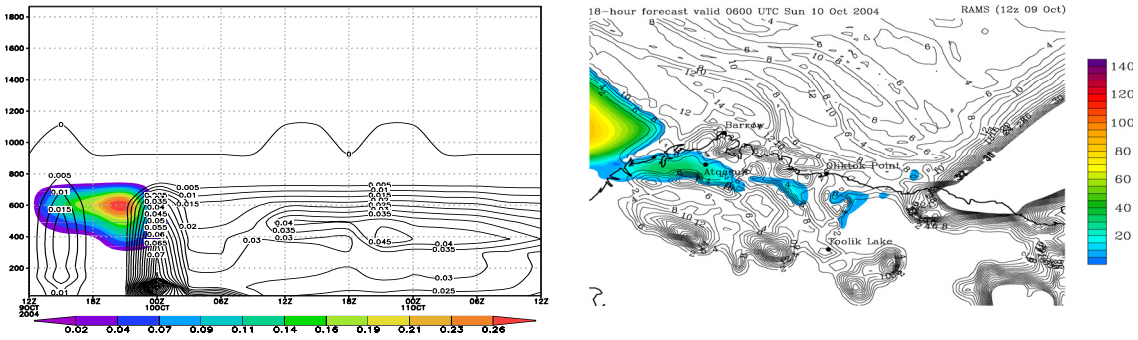

a) **b)**

Figure 3.6: **(a)** Time evolution of the liquid (shaded) and ice (contoured) water mixing ratio [g/kg] over Barrow, and **(b)** liquid (shaded) and ice water path (contoured) [g m^{-2}] at 18 hours of simulation time for the "base run"

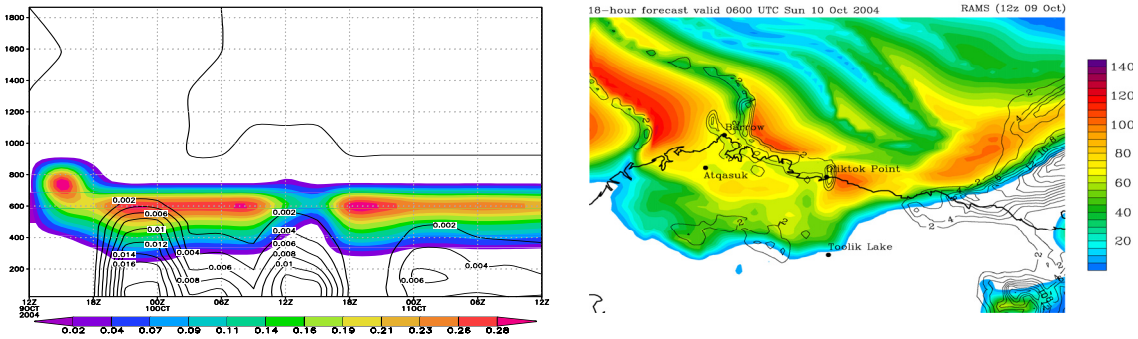

a) **b)**

Figure 3.7: **(a)** Time evolution of the liquid (shaded) and ice (contoured) water mixing ratio [g/kg] over Barrow, and **(b)** liquid (shaded) and ice water path (contoured) [g m^{-2}] at 18 hours of simulation time for the "MPACE IN" run

of which then precipitates (Figure 3.6a). In contrast with observations, 18 hours after the beginning of the simulation the cloud liquid water throughout most of the domain of grid #2 is almost completely depleted and the region is covered by thin ice clouds (Figure 3.6b). Simulated liquid water path (Figure 3.8a) is significantly lower than the observed one. Results from this run appear to be similar to those produced by the ARCMIP models during winter months.

The same simulation was then repeated using a new deposition/condensation-freezing IN parameterization, derived from the “in-situ” IN measurements collected during M-PACE (Prenni et al., 2007). This new parameterization has the same functional form as Meyers et al. (1992) but the predicted IN concentrations are approximately 26 times lower. Since we did not have contact nucleation measurement data, we assumed that the IN available for contact nucleation must be reduced by the same factor as deposition/condensation-freezing IN. When these lower, but more realistic values of the IN concentration were used in the new simulation, the cloud structure drastically changed. A persistent stratus cloud layer with smaller amounts of ice is produced. As illustrated on Figure 3.7a and b, the liquid and ice coexist throughout the entire simulation in better agreement with observations. Simulated liquid water path is underestimated in the first half of the simulation period but follows the observed LWP very well after that (Figure 3.8a). Despite this disagreement, the new simulation represents a significant improvement over the standard IN case (Standard IN).

Another two simulations, in which deposition/condensation-freezing IN were increased by a factor of two (2xMPACE IN) and ten (10xMPACE IN), were performed to examine the sensitivity of the simulated mesoscale cloud fields to IN concentration.

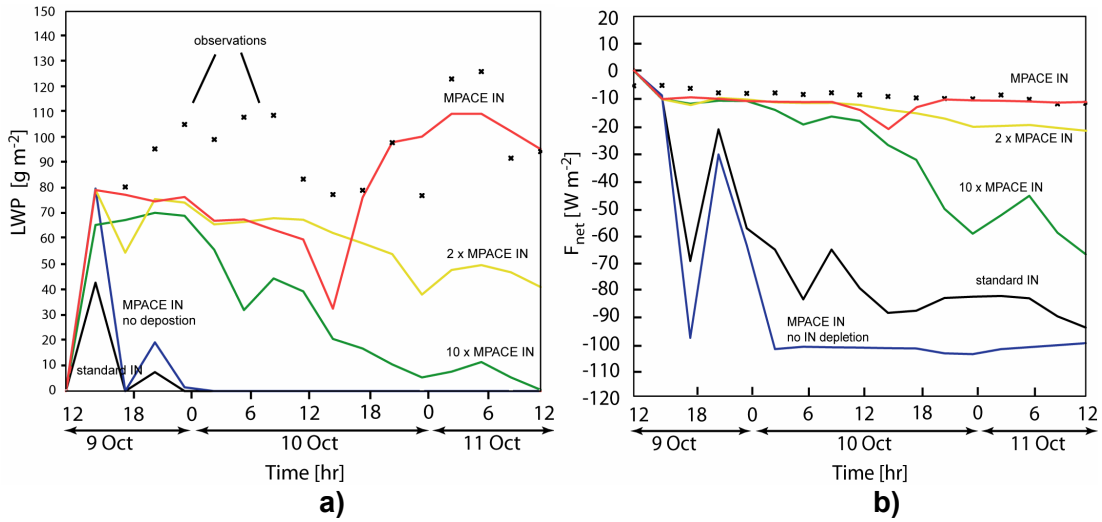

Figure 3.8: **(a)** Simulated and observed (symbols) liquid water path [g m^{-2}] and **(b)** net longwave radiative flux [W m^{-2}] at Oliktok point for different sensitivity runs: base run (black), M-PACE derived IN parameterization (red), two times increased IN concentration (magenta), 10 times increased IN concentration (green), diagnosed IN (dark blue).

While both simulations are still able to maintain a mixed-phase cloud deck, the liquid phase gradually decreases as the IN concentrations increase (Figure 3.8 a). In all simulations above, both deposition/condensation-freezing and contact IN are depleted (prognosed) due to ice crystal nucleation and precipitation. When the depletion of IN is turned off (MPACE IN, No Depletion), even the MPACE-derived IN concentrations caused a rapid glaciation, which is consistent with the previous studies of Harrington and Olsson (2001a) and Morrison et al. (2005).

Correctly simulating mixed-phase clouds is important for many reasons, but one of the most important reasons is the influence of these clouds on the Arctic radiation budget. Figure 3.8b shows the net infrared radiative flux at the surface for each simulation shown in Figure 3.8a. The simulation with the new IN parameterization and IN depletion (MPACE IN) compares very well with surface observations of downwelling and upwelling broadband longwave radiation. This is because the liquid phase dominates the radiative budget, so any simulation that maintains a large fraction of liquid will tend to have a relatively accurate surface infrared radiative budget. As IN concentrations increase in the model, liquid water is converted rapidly to ice, leading to optically thin clouds. This causes the net infrared radiative loss to change dramatically. Thus, small changes in the IN population, and whether or not IN are depleted in the model, can lead to substantial changes in the surface radiative budget (up to 100 Wm^{-2}). These results match the prior results of Harrington and Olsson (2001b).

Morrison et al. (2005) suggested a conceptual model of Arctic mixed-phase clouds that explains the cloud persistence through the rapid depletion of deposition/condensation-freezing nuclei and a self-regulating negative feedback involving drop freezing by contact nucleation. In their simulations, the continual ice production was due primarily to contact nucleation mechanism. To examine the sensitivity of the simulated clouds to the contact IN parameterization in our model, and so compare to Morrison et al. (2005), simulations with concentrations of IN available for contact nucleation from 26 times lower (assumed M-PACE contact IN concentrations) to 1000 times higher than those predicted by Meyers

et al. (1992) were conducted. The deposition/condensation-freezing IN concentration was set to the M-PACE observed values in these simulations.

Simulated liquid water path for all sensitivity runs is shown in Figure 3.9. In contrast to the previous experiment (where the sensitivity to deposition/condensation-freezing IN concentration was examined), despite the wide range of contact IN concentrations, no significant sensitivity to contact IN

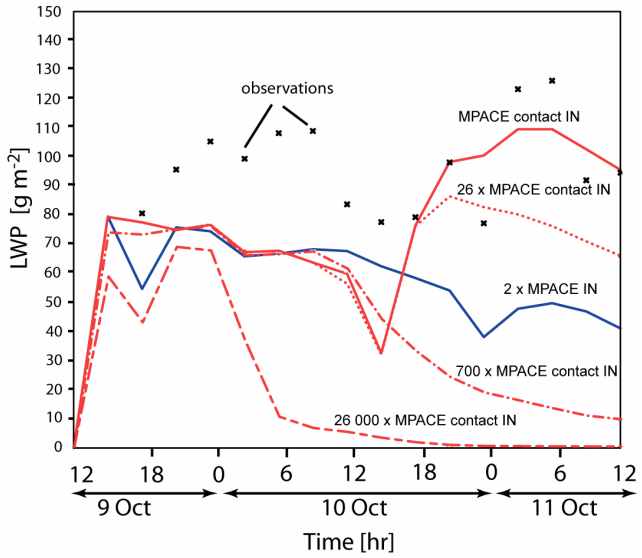

Figure 3.9: Simulated and observed (symbols) liquid water path [gm^{-2}] at Oliktok point for different contact IN sensitivity runs: M-PACE derived IN parameterization (solid red), 26 times increased contact IN concentration (dotted red), 700 times increased contact IN concentration (dash-dotted red), 26 000 times increased contact IN concentration (dashed red), two times increased deposition/condensation-freezing IN concentration (blue).

was found. Simulation with 26 times increased contact IN concentration (26xMPACE contact IN) practically overlaps the “base” run (MPACE contact IN) for most of the simulation period. Increasing the contact IN concentration up to 700 times (700xMPACE contact IN) leads to a gradual decrease of the simulated liquid water path in the second half of the simulation. Note that a similar reduction

in the simulated LWP could be obtained by increasing the deposition/condensation-freezing IN concentration by only a factor of two (2xMPACE IN in Figure 3.9), as opposed to 700 times increase in the case of contact IN. Liquid water is sustained in the simulated cloud layer even for the unrealistic case of contact IN concentration increased 26 000 times (26 000xMPACE contact IN).

Nucleation rates and number of ice crystals produced by deposition/condensation-freezing and contact nucleation are presented in Figure 3.10. The comparison reveals that contact IN concentrations should be increased

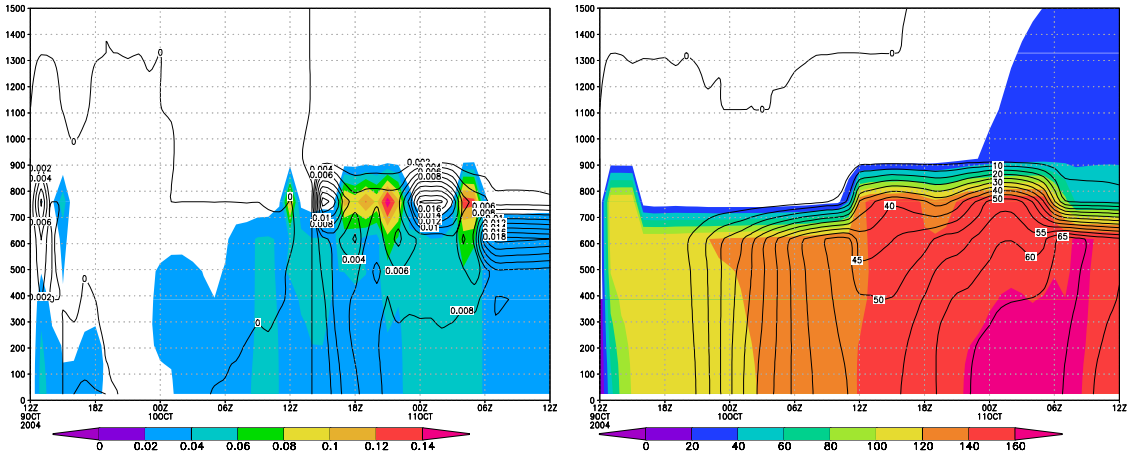

a) **b)**

Figure 3.10: **(a)** Deposition/condensation-freezing (shaded) and contact (contoured) nucleation rates [$m^{-3}s^{-1}$], and **(b)** the number of IN per m^3 depleted since the beginning of simulation through deposition/condensation-freezing (shaded) and contact nucleation (contoured) for simulation with 700 times increased available contact IN.

at least 700 times in order for contact nucleation to produce nucleation rates and number of ice crystals comparable to those produced by deposition/condensation-freezing nucleation. For contact IN concentrations, that

we assumed to be appropriate for the M-PACE conditions and used in our best simulation (MPACE contact IN in Figure 3.9), contact nucleation rates and number of ice crystals produced (not shown) are about three orders of magnitude lower than those of deposition/condensation-freezing nucleation.

In the absence of surface sources of IN, after the initial depletion of the boundary layer IN, the only remaining mechanisms for ice production are contact nucleation, entrainment of IN from the layers above during cloud deepening in response to surface fluxes and vertical and horizontal transport of IN by locally induced circulations. As we already showed, the contact nucleation is not an effective ice producing mechanism, at least in the case we simulated. Evidence suggests that coastally induced mesoscale circulations might be important for maintaining the continuous ice production in mixed-phased clouds along the coast. Indeed, as Figure 3.7b shows, ice precipitation bands form along the coast.

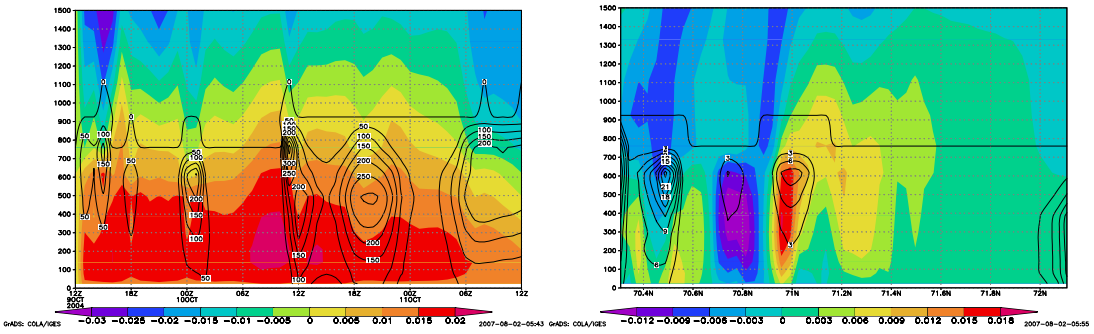

(a) **(b)**

Figure 3.11: **(a)** Vertical velocity [m/s] (shaded) and pristine ice concentration [#/m^3] (contoured): time series at Barrow and **(b)** N/S vertical cross-section of grid #3, shoreline is between 70.8N and 71N (b)

The effect of IN entrainment and IN transport by coastal circulations is illustrated on Figure 3.11. The bursts in pristine ice concentration field around 15Z, 0Z, 18Z and 06Z (Figure 3.11a) are very well correlated with the negative peaks in the vertical velocity field, i.e. they can be explained by vertical intrusions of IN from the layers above. The peak at 12Z can be attributed to both vertical transport and deepening of the cloud layer. The first two peaks onshore (Figure 3.11b) are also related to downdrafts, while the peak over the ocean is associated with the increase of supersaturation in the mesoscale updraft, and subsequent IN activation. Coastal dynamics effects are also illustrated on Figure 3.12 showing simulated mean vertical velocity, liquid water path and number of

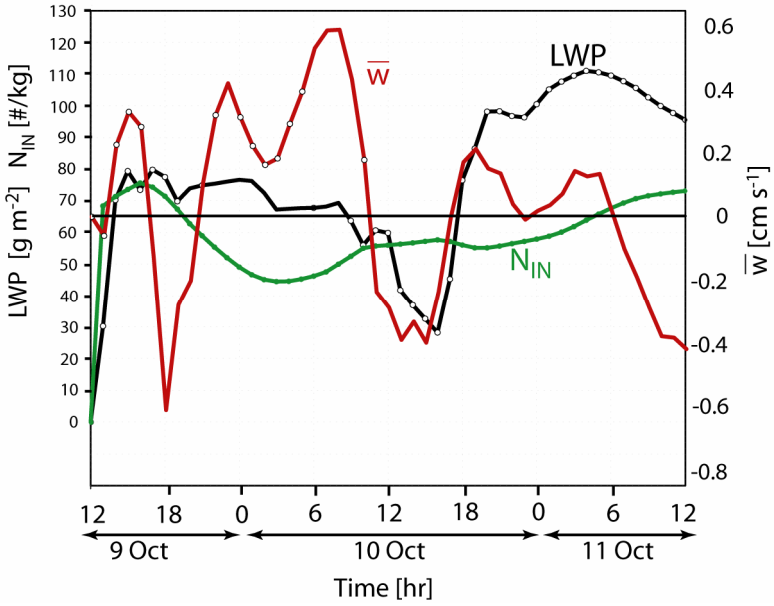

Figure 3.12: Mean vertical velocity [cm/s] (red), number of activated deposition/condensation-freezing IN [#/m^3] (green) and liquid water path [gm^{-2}] (black) at Oliktok point

activated deposition/condensation-freezing IN at Oliktok point. As Figure 3.12 shows, mesoscale updrafts are associated with higher LWP, lower number of

activated IN and consequently, weaker snow precipitation. Downdrafts, on the other hand, transport IN-reach air from aloft, causing rapid pristine ice production and enhanced Bergeron process leading to LWP decrease and stronger snow precipitation.

3.4 Summary

In this chapter we investigated the influence of IN concentrations and ice nucleation modes on the structure and life-time of simulated Arctic mixed-phase clouds. Using IN parameterization derived from “in-situ” IN measurements results in a realistic mixed-phase cloud layer, very similar to the observed one. In contrast, when IN concentrations typical for mid-latitudes are used, the cloud layer rapidly glaciates. Our results show that the structure and the lifetime of simulated Arctic mixed-phase clouds is highly sensitive to deposition/condensation-freezing IN and shows almost no sensitivity to the number of IN available for contact nucleation. In our simulations contact nucleation mode could not produce significant ice water amounts unless the ambient contact IN concentrations were increased to unrealistically high values. As a consequence of that, we find the deposition/condensation-freezing nucleation to be the dominant, controlling heterogeneous nucleation mode.

In addition, we find that local, coastally induced mesoscale circulations are responsible for maintaining the continuous ice precipitation along the coastline. Results from our sensitivity tests suggest that in order to correctly simulate Arctic

mixed-phase stratus clouds, models must correctly predict not only the number of heterogeneously nucleated ice crystals but also the cloud processing and removal of IN through precipitation. While the lower sensitivity to contact IN is consistent with results of previous studies (e.g. Harrington et al., 1999; Harrington and Olsson, 2001a; Morrison et al., 2005) our conclusion about the dominant role of deposition/condensation-freezing nucleation contradicts Morrison et al. (2005) and Morrison and Pinto's (2005) findings and requires further investigation.

Results from the simulations, presented in this chapter, support the notion that the phase of water in Arctic boundary layer clouds plays a critical role in Arctic regional climate. Further, in comparison with those of the ARCMIP simulations, these results suggest that the lack of liquid water in Arctic clouds predicted by models, and hence the errors in the surface radiative budget, is possibly linked to inadequate parameterizations of ice processes, and ice nuclei, in the Arctic.

Chapter 4

The influence of parameterized ice habit on the longevity of mixed-phase Arctic stratus

While all prior studies focus primarily on ice nucleation and ice concentrations, it is also possible that ice habit and how it is parameterized affects the microphysical structure of mixed-phase Arctic stratus. Liquid water evaporation by ice crystals depends not only on ice concentration but also on ice in-cloud residence time and mass growth rate. The in-cloud residence time is inversely proportional to the sedimentation velocity of the crystals, which is controlled by their habit and size (Eq. 2.6). The mass growth rate (Eq. 2.7) through mass-dimensional relation (Eq. 2.9) and shape parameter also depends on the habit of the crystals. Hence, the phase partitioning of mixed-phase stratus may depend significantly on how the habit of the crystals is parameterized. Indeed, in a simplified example, Harrington et al. (1999) showed that changing ice habit may have a substantial effect on mixed-phase cloud evolution. Moreover, many models use different parameterizations for crystal habit, which may lead to substantial differences in the final model results. In this chapter, we examine the influence that ice habit may have on the simulated evolution of mixed-phase Arctic stratus.

4.1 Case description

In this study, we focus on two periods from M-PACE (Verlinde et al., 2007) - the period from 12 Z on October 5 to 12 Z on October 8 and the period from 17 Z on October 9 to 5 Z on October 10, 2004. These two periods were selected because of the different environmental and synoptic conditions which lead to different cloud conditions – a single mixed-phase cloud layer (Period B Oct. 9-10, Klein et al., 2008) and multiple liquid layers with ice crystals falling between them (Period A Oct. 5-8, Morrison et al., 2008b).

During the period A (Oct 5-8) the synoptic situation was characterized by a high pressure center developing over the sea-ice to the northeast of the northern Alaska coast (Fig. 4.1a). A small, mid-level low pressure center moved along the northern coast of Alaska, bringing significant amounts of mid- and upper-level moisture and producing multiple-layered supercooled liquid clouds (Verlinde et al., 2007). The mid-level disturbance, and the cloud layers, dissipated on October 7. During period B (Oct 9-10), the high pressure center over the sea-ice intensified and together with surface Aleutian low, created a significant pressure gradient over the area (Fig. 4.1b). This produced strong northeasterly winds moving cold air (~ -20 °C) from the sea-ice and over the relatively warm ocean surface producing single-layered mixed phase boundary layer clouds and rolls (see Fig. 3 in Verlinde et al., 2007). A detailed description of the synoptic processes is given by Verlinde et al. (2007) and Yannuzi (2007).

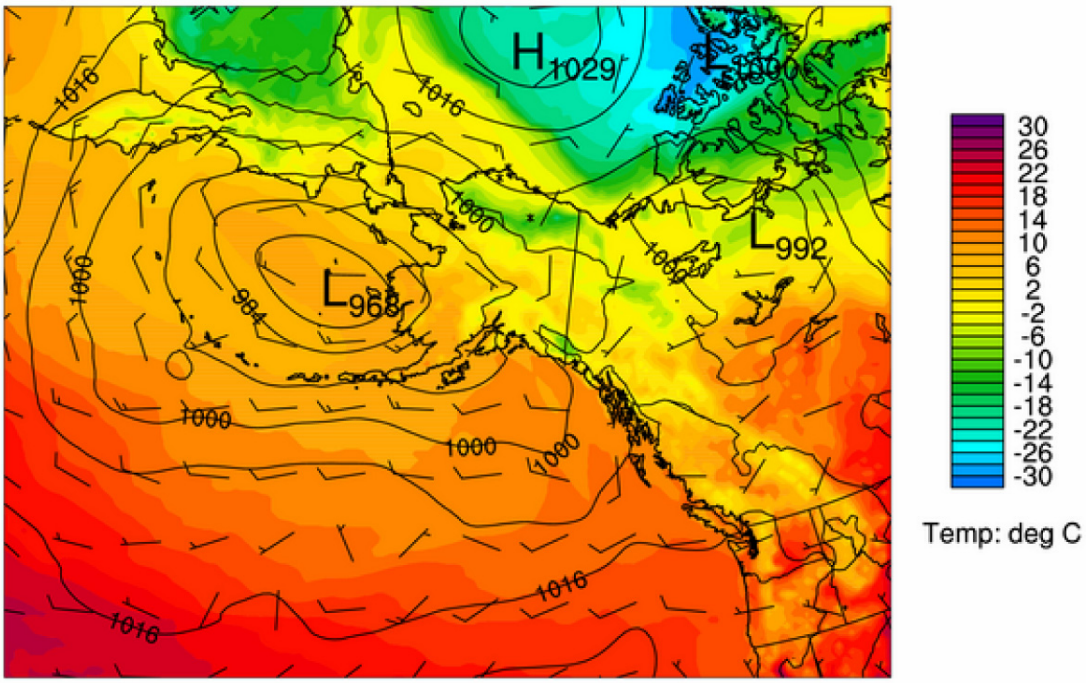

a)

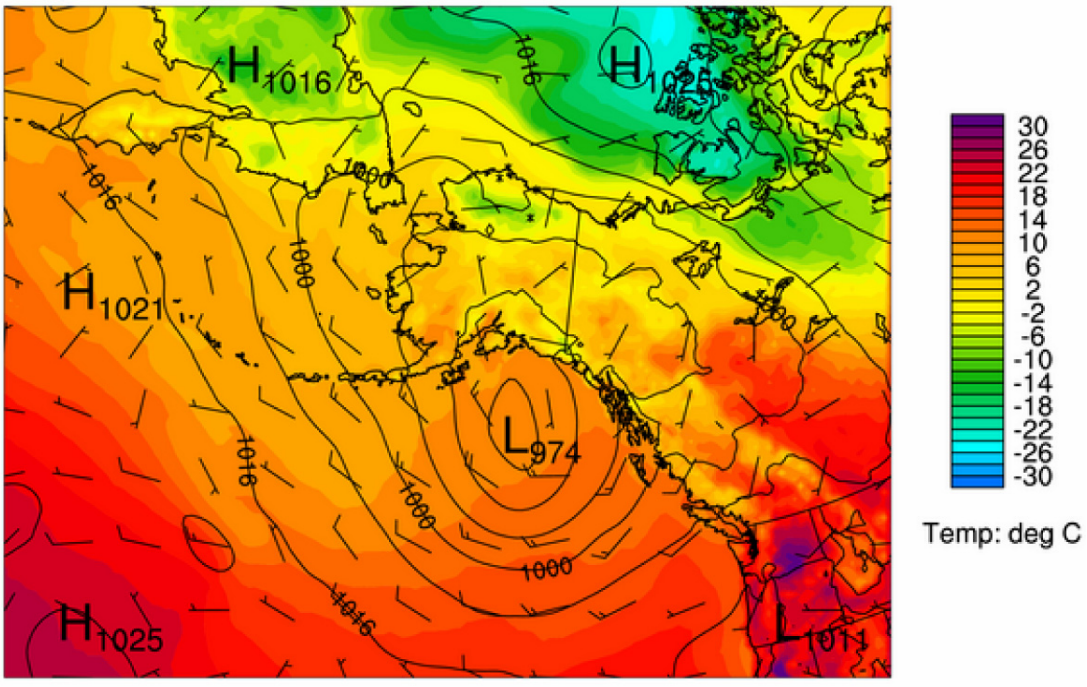

b)

Figure 4.1: ETA surface analysis valid for **(a)** 00 UTC 6 October 2004 and **(b)** 00 UTC 10 October 2004. Shown are air temperature (shaded), mean sea level pressure (contoured) and surface wind (barbs).

4.2 Model setup and simulation design

The model was configured as a two-dimensional cloud-resolving model for the M-PACE Intercomparison studies (Klein et al., 2008; Morrison et al., 2008b). The computational domain has 150 horizontal grid points with 1 km spacing and 72 vertical grid points with 25 m spacing in the boundary layer, stretching to 1000 m at the domain top. The model is initialized with a prescribed sounding and constant winds, large scale forcing and surface fluxes, developed specifically for the M-PACE model inter-comparison study. The soil-vegetation and sea-ice submodels of RAMS were not used in this study and the lower boundary is assumed to be snow covered land (case A) or ocean surface (case B). The duration of the case A simulation is 72 hours and case B is 12 hours, with a 2 second time-step.

This study was motivated in part by the fact that some studies show faster glaciation (Harrington et al., 1999) as compared to others (Morrison et al., 2008a; Fridlind et al., 2007). To investigate the influence of parameterized ice crystal habit on simulations of mixed-phase clouds we performed a series of sensitivity runs in which we used different ice crystal shapes. Three basic crystal shapes were used in these simulations – hexagonal plates, dendrites and spheres. There are several reasons why we selected these crystal habits. First, the observed temperature and supersaturation ranges in both cases favor depositional growth of dendrites and hexagonal plates. The spherical shapes were included, in part, because they produce the smallest possible size for a given mass and so provide the strongest contrast to dendrites, which have the largest size for a given mass.

Spheres also have the largest fall speed for a given mass. Second, inclusion of spheres allows us to directly compare our results to those of Morrison et al. (2008a) and Fridlind et al. (2007), who used spherical shapes in their simulations.

Each crystal shape is characterized by its own mass-dimensional and terminal velocity relationships, as well as shape parameters. The relationships reported in the literature for non-spherical ice span a relatively large range (Pruppacher and Klett, 1997; Mitchell, 1996; Heymsfield and Kajikawa, 1987; Heymsfield et al., 2002) and these are used in models. However, model simulations of mixed-phase clouds are likely sensitive to the mass-dimensional relation used. Hence, we examine the sensitivity of model-simulated mixed-phase clouds to mass and fall speed relations. For spheres we use similar relationships to those of Fridlind et al. (2007) and Morrison et al. (2008a) (formula from personal communication).

Figure 4.2a and Figure 4.2b show the ranges of variation of the mass-dimensional and terminal velocity relationships. For our simulations, we select relations that define the maximum and minimum for each mass and fall-speed range. The sensitivity of the simulated cloud with respect to crystal habit is then investigated using these extremes. In our work we use the terms “large” and “small” to indicate the extremes in the mass-dimensional relation that produces maximum and minimum size, respectively, for a given crystal mass. Similarly, “fast falling” and “slow falling” will denote the use of the terminal fall velocity relation producing maximum and minimum sedimentation velocity, respectively,

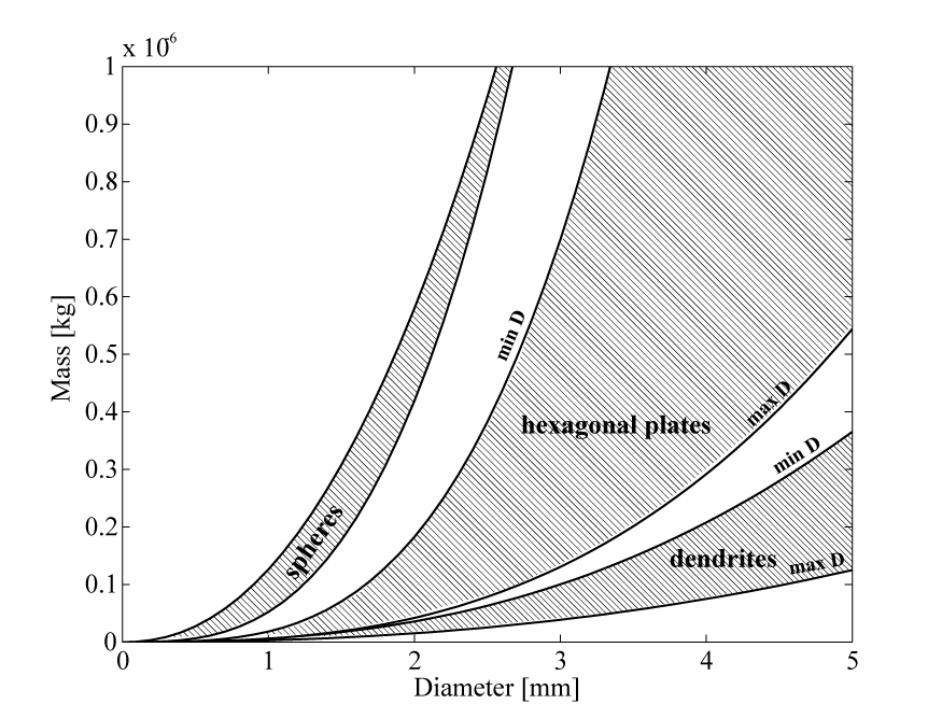

a)

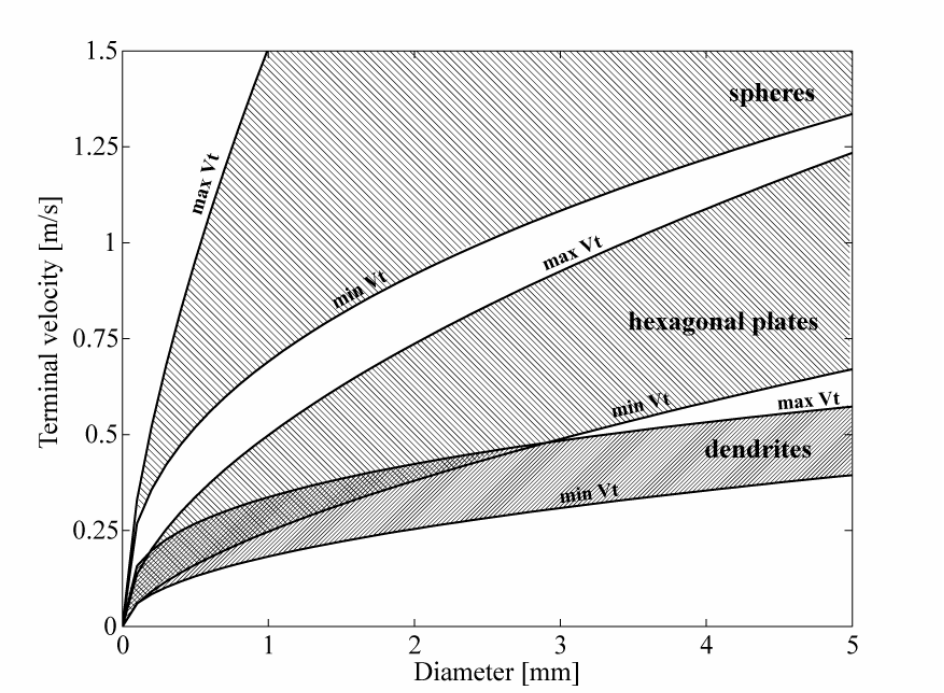

b)

Figure 4.2: Ranges of **(a)** mass-dimensional and **(b)** terminal velocity relations for crystal habits used in the simulations.

for a given crystal diameter (see Fig. 4.2a and 4.2b).

Crystal capacitance in RAMS, and in other models as well, is specified as a function of crystal maximum dimension D multiplying a constant shape parameter S, which has a different value for each crystal habit. While analytical forms of the shape parameters of spheres and spheroids exist (e.g. Chen and Lamb, 1994), the shape parameter of dendritic and hexagonal shapes must be computed numerically (Westbrook et al., 2008). Because S is fixed, but ice growth depends non-linearly on S (Chen and Lamb, 1994), we included a series of runs where the shape parameter of dendrites was varied from the baseline value of 0.31 down to 0.22 (see Fig. 11 in Westbrook et al., 2008). For hexagonal plates we assumed a shape parameter of a thin circular disk (0.31) and for spherical crystals the shape parameter was set to 0.5.

4.3 Results

4.3.1 *Single layer cloud, comparison with observations*

In our baseline series of simulations we used dendritic crystal shapes because RAMS choses this shape given the ambient temperature and supersaturation of the cloud; moreover, this shape was used in the mesoscale simulations of Prenni et al. (2007), who simulated the same case. Simulations were done using various combinations of the upper and lower limits of the mass-dimensional and fall velocity relations (Fig. 4.2), creating four different dendritic crystal classes: large, slow falling; large, fast falling; small, slow falling and small, fast falling. By using combinations of the extremes in the mass and fall-speed

relations (Fig. 4.2) our simulations span the range of cloud sensitivity to the way crystal habit is parameterized in a bulk microphysical model.

The best match with the observed liquid and ice water path, averaged for the simulation period, was obtained in the case of small, fast falling dendrites (Fig. 4.3a and 4.3b). The other three combinations produced either too low of a liquid water path (LWP) (large, fast and slow falling) or higher LWP and too low of a ice water path (IWP) (small, slow falling). Liquid water path observational data are derived from microwave radiometer measurements (Turner et al., 2007) and are averaged for the three sites available – Atqasuk, Barrow and Oliktok Point. Unfortunately, no ice water path data were available, so the estimated range of IWP from Klein et al. (2008) was used.

During the simulation period the observed LWP shows almost regular oscillations between 90 and 170 g/m^2. The overall simulated LWP tends to remain within the observed range and, except for the beginning of the simulation, the oscillations in the liquid water path follow the observations remarkably well. The troughs in simulated LWP are correlated with peaks in the simulated IWP (Fig. 4.3b). An analysis of the simulation showed that these IWP peaks are caused by entrainment of IN-rich air from above the cloud layer, producing ice precipitation streaks leading to a decrease of the liquid (similar to Carrio et al., 2005). The IN depletion through sedimentation of the cloud layer by precipitation then allows for a consequent liquid increase (Harrington and Olsson, 2001a). Since no ice water path data were available, a detailed comparison with the observations was not possible. However, the simulated IWP is below estimated

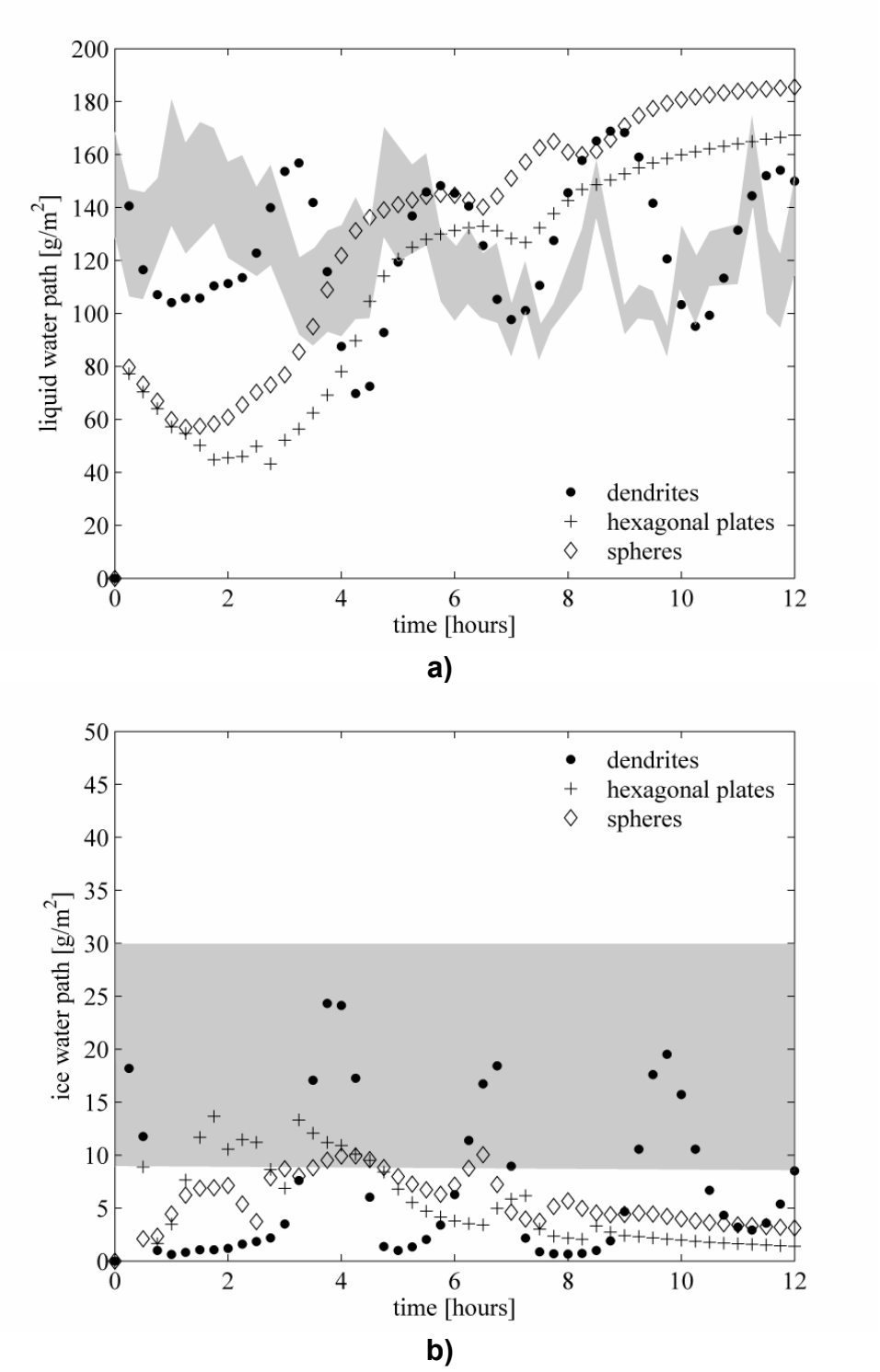

Figure 4.3: Time series of simulated (symbols) and retrieved (shaded) **(a)** liquid and **(b)** ice water path [gm^{-2}]: single layer case. Simulated quantities are domain averaged. Shaded area in **(a)** represents 95% confidence interval of observational data and ice water path estimate of Klein et al. (2008) in **(b)**.

range of observed IWP, except during the precipitation periods (Fig. 4.3b).

The averaged profiles of simulated liquid and ice water content (LWC and IWC) are compared to aircraft observations on Figure 4.4a and 4.4b. Measurement data are from flight 10a (McFarquhar et al., 2007) and modeled quantities are averaged over the flight duration. Simulated LWC is slightly lower than the observations in the lower half of the cloud layer, but the match is better near cloud top (Fig. 4.4a). Predicted IWC, however, is significantly underestimated with a difference of about a factor of 2 inside the cloud layer and about a factor of 10 below the cloud base (Fig. 4.4b). This is due primarily to the depletion of IN by nucleation-scavenging (c.f. Fridlind et al., 2007).

Though the simulation using dendrites compares well with the observed LWP, this is somewhat fortuitous because, as we shall show, the results depend critically on the mass and fall-speed relations chosen.

In addition to simulations with dendrites, we performed two series of simulations using spheres and hexagonal plates. Both series of runs, however, showed similar results – a predominantly liquid cloud layer with essentially no ice, which is in contrast to the observations. The only way the simulated liquid and ice water path could be brought into the range of observations was to increase the IN concentration by a factor of 25, up to the values typical for mid-latitudes. Hence for more compact, slower growing, faster falling hexagonal plates and spheres higher IN concentrations are needed to produce a better match with observations (Fig. 4.3a and 4.3b). We should note that a similar increase of the IN concentration in simulations with dendrites led to almost

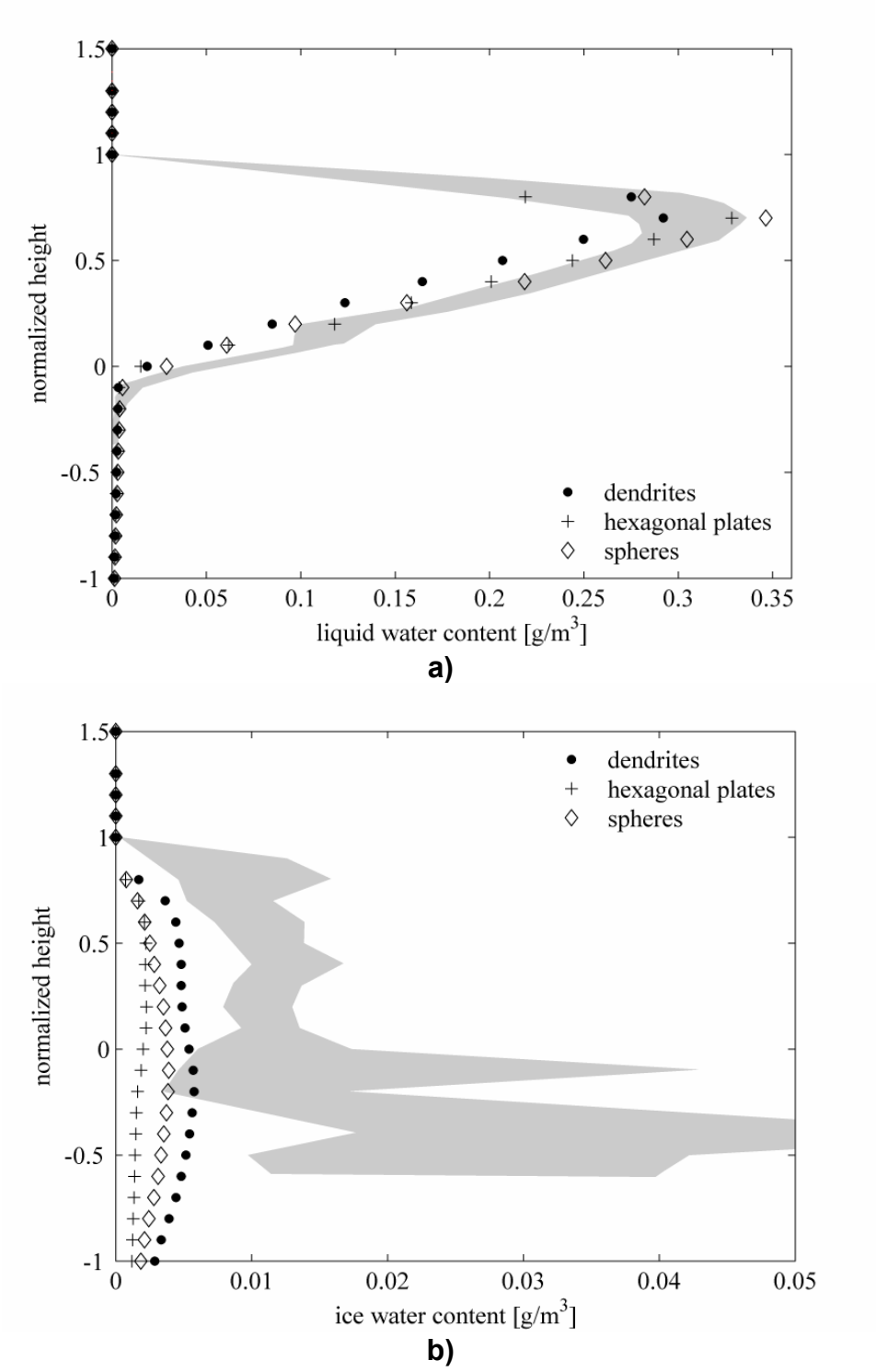

Figure 4.4: Time-averaged vertical profiles of **(a)** simulated domain averaged (symbols) and observed (shaded) liquid and **(b)** ice water content [gm^{-3}]: single layer case. Simulated and observed quantities are averaged over the flight duration. Shaded area represents 95% confidence interval of observational data.

complete glaciation of the simulated cloud layer which is similar to prior results (Harrington and Olsson, 2001a; Prenni et al., 2007).

Although both the simulation-averaged ice and liquid water paths are similar for all three crystal habits, the time evolution shows considerable differences. Only the simulation using dendrites is capable of adequately capturing the oscillations in the observed liquid water path. Although simulations with spheres and hexagonal plates produced a similar dynamical structure and entrainment rates (not shown), the slower depositional growth of hexagonal and spherical ice leads to a different temporal evolution of the liquid and ice water paths. Despite the higher ice concentrations in these simulations in comparison to dendrites, the IWP in all three simulations is well below the range of observational data. Liquid water profiles in simulations using hexagonal plates and spheres show better agreement with the observed profile than dendrites (Fig. 4.4a) and the ice water content is significantly underestimated in all three simulations (Fig. 4.4b).

4.3.2 *Single layer cloud: Habit sensitivity*

The different concentrations of ice needed to match observations in the simulations above motivated us to examine the influence of the choice of ice crystal habit (mass-dimensional, terminal fall velocity relationships and capacitance) on phase partitioning in mixed-phase clouds. Moreover, Prenni et al. ‘s (2007) results show a much stronger sensitivity to IN concentration than either Morrison et al. (2008a) or Fridlind et al. (2007). To explore habit sensitivity

we performed four series of simulations using combinations of the lower and upper limits of the mass-dimensional and terminal fall velocity relations for each habit. In each series of simulations, the IN concentration was varied from the value measured during M-PACE (0.15/L, we define as a relative IN concentration of one) up to a value 50 times larger (approximately twice the Meyers et al., 1992 formulation, relative IN concentration of 50). Spherical crystals were used to compare with other studies that used spheres (Fridlind et al., 2007; Morrison et al., 2008a).

In order to show the overall influence of habit on simulated phase-partitioning, we computed simulation-averaged LWP and IWP for all IN concentrations and for each simulation. The results are summarized on Figure 4.5a and Figure 4.5b, showing the range of the liquid and ice water path produced by varying the mass and terminal fall speed relation for each habit as a function of IN concentration (see Table 4.1 for details). The simulations shown on Figure 4.3 and 4.4 are denoted with a star in Table 4.1.

Simulations with hexagonal plates and spherical shapes produced similar results, though with a different spread. The liquid water path was the greatest and the ice water path the smallest for these habits. At low IN concentrations both hexagonal plates and spheres do not show much sensitivity to the mass-dimensional and terminal fall velocity relations. As the IN concentration increases, however, the range of liquid and ice water path variation also increases, reaching relative differences of up to 60% and 75% for the liquid and ice water path, respectively. The upper and lower bounds of the LWP range are

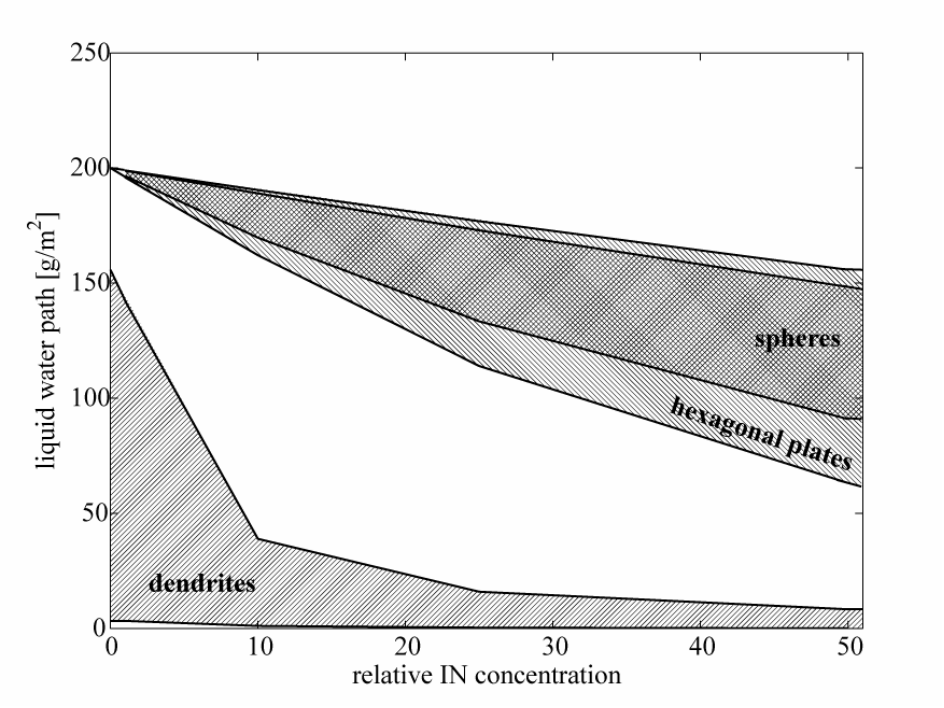

a)

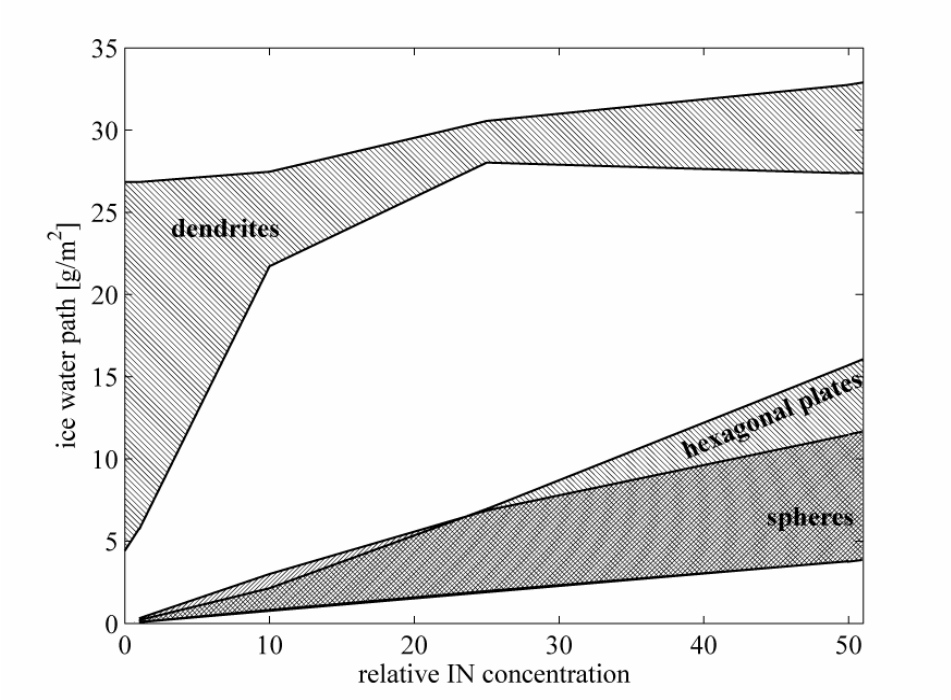

b)

Figure 4.5: Ranges of simulated **(a)** liquid and **(b)** ice water path [gm^{-2}] for different habits as a function of IN concentration: single layer case. Simulated quantities are domain and simulation averaged. IN concentration is relative to $0.15L^{-1}$.

defined by simulations using small, fast-falling habits and large, slow-falling habits respectively.

Simulations using small and fast-falling hexagonal plates or spheres produced the largest liquid and smallest ice water path and conversely, the use of large and slow-falling hexagonal plates led to lowest liquid and highest ice water path. Physically, this makes sense because smaller particles have lower overall mass growth rates. If these crystals are then removed quickly, more liquid can be maintained. Note that spheres tend to define the upper limit: they are the smallest, fastest falling particles. The combinations of maximum size/maximum

Table 4.1: Observed and simulated liquid and ice water path as a function of IN concentration: single layer case. Simulated quantities are domain and simulation averaged.

M-D	Vt	LWP [g/m^2] at relative IN concentration of				IWP [g/m^2] at relative IN concentration of			
		x1	x10	x25	x50	x1	x10	x25	x50
				Dendrites					
max D	min Vt	24.3	9.5	1.0	0.3	19.7	22.9	24.2	24.5
max D	max Vt	3.3	1.1	0.4	0.0	26.8	27.5	26.9	28.1
Min D	min Vt	125.9*	38.9	16.0	8.3	7.0*	21.7	30.6	32.7
Min D	max Vt	142.3	26.3	11.1	4.2	5.7	23.9	28.0	27.4
				Hexagonal plates					
max D	min Vt	195.9	162.1	114.0*	63.1	0.2	2.1	7.0*	15.7
max D	max Vt	197.8	180.8	155.1	120.6	0.1	0.9	2.4	5.3
Min D	min Vt	197.7	178.9	165.1	118.1	0.2	2.1	4.5	10.9
Min D	max Vt	198.9	190.4	176.9	155.8	0.1	0.8	1.9	3.8
				Spheres					
Min D	max Vt	198.8	189.0	172.9	148.3	0.1	0.8	2.0	3.8
max D	min Vt	196.6	169.7	133.3*	90.9	0.3	3.0	6.9*	11.5
				Observations - Klein et al. (2008)					
Airborne		115				7.6			
Ground based		107-210				29.4			

fall velocity and minimum size/minimum fall velocity produced virtually identical liquid water paths (Table 4.1). The sensitivity to IN concentration is also dependent on the chosen mass-dimensional and fall velocity relations. The change in liquid water path with a relative IN increase from one to 50 for larger and slow falling hexagonal plates is 68%, as compared to only 22% in the case of smaller, faster falling plates.

In contrast to experiments with hexagonal plates and spheres, simulations with dendrites showed much stronger IN sensitivity. Unlike hexagonal plates, liquid and ice water paths for dendritic crystals depend strongly on the mass-dimensional relation used, and much less on the terminal fall speed formulation. At very low IN concentrations (< 1 L^{-1}) simulations with small (slow-growing) dendrites produced a mixed-phase cloud layer continuously precipitating ice, similar to what simulations with spheres and hexagonal plates produced. The liquid water path is also comparable to that of hexagonal plates and spheres. Increasing the IN concentration up to the values typical for mid-latitudes, however, leads to a large reduction in the LWP, similar to what has been reported in prior studies with dendrites (Harrington, 1997; Harrington and Olsson, 2001a; Jiang et al., 2000; Prenni et al., 2007). In the case of large (fast-growing) dendrites, the amount of liquid water is negligible even at low IN concentrations.

The large range of sensitivity for dendrites also makes physical sense. Dendritic crystals have the largest increase in growth rate with increase in maximum dimension (e.g. Chen and Lamb, 1994; Sheridan, 2008). Consequently, dendritic growth is quite sensitive to the mass-dimensional

relationship choices, leading to a wide range of possible LWP and IWP (Fig. 4.5). The range is greatest at low IN concentrations because crystal sizes are largest here, leading to the strongest growth, and hence the largest sensitivity to mass-dimensional relations.

Many models constrain crystal habit by using mass and fall-speed relations like the ones used here. Consequently, the range of the predicted LWP and IWP in a model appears to depend greatly on this choice. For instance, the studies of Harrington and Olsson (2001a) and Prenni et al. (2007) used dendritic crystals and showed a strong sensitivity to IN concentration. In contrast, Morrison et al. (2008) and Fridlind et al. (2007) studies are much less sensitive to IN concentration and both used spheres in their simulations. However, our simulations show that almost any range of LWP and IWP can be produced by judicious choice of mass and terminal fall speed relations. Furthermore, precisely because of the large potential range of LWP and IWP, it appears that simulating changes in crystal habit is of vital importance for simulations of mixed-phase clouds. At present, no cloud model attempts to predict realistic habit change and so results are constrained to lie somewhere in the parametric map given by Figure 4.5.

4.3.3 Multi-layered clouds

Analogous results to the single layer case were obtained for the multi-layered case. The ranges of liquid and ice water paths for each crystal habit are shown in Figure 4.6a and 4.6b, and results from all simulations are shown in

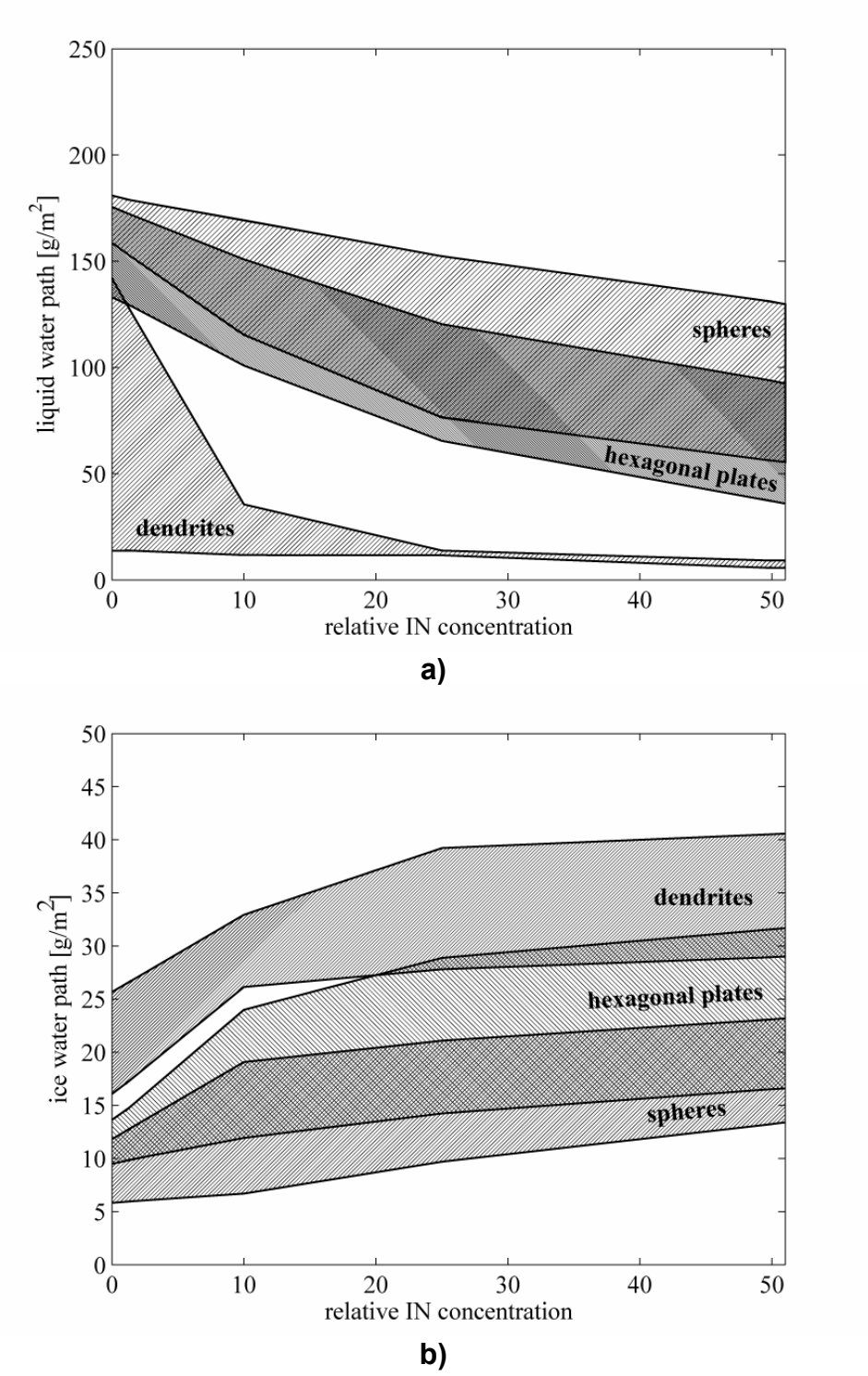

Figure 4.6: Ranges of simulated **(a)** liquid and **(b)** ice water path [gm^{-2}] for different habits as a function of IN concentration: multi-layered clouds case. Simulated quantities are domain and simulation averaged. IN concentration is relative to $0.15L^{-1}$.

Table 4.2: Observed and simulated liquid and ice water paths as a function of IN concentration: multiple layers case. Simulated quantities are domain and simulation averaged.

M-D	Vt	LWP [g/m^2] at relative IN concentration of				IWP [g/m^2] At relative IN concentration of			
		x1	x10	x25	x50	x1	x10	x25	x50
				Dendrites					
max D	min Vt	30.6	10.1	6.1	6.7	25.4	26.1	27.9	30.1
max D	max Vt	13.9	11.8	11.6	5.7	26.4	26.5	27.8	28.9
min D	min Vt	131.0	35.6	13.9	8.9	17.0	32.9	39.2	40.5
min D	max Vt	118.3*	20.2	12.7	9.1	17.2*	31.3	30.9	33.0
				Hexagonal plates					
max D	min Vt	130.4	100.9	65.5	37.0	13.1	17.5	21.7	27.4
max D	max Vt	143.9	117.4	89.0*	59.5	9.8	11.9	14.2*	16.5
min D	min Vt	155.8	122.7	95.5	72.5	14.5	24.0	28.9	31.6
min D	max Vt	172.9	154.9	118.8	96.0	10.8	12.9	17.3	20.7
				Spheres					
min D	max Vt	179.2	169.3	152.3	131.0	5.9	6.7	9.7	13.2
max D	min Vt	154.1	115.4	76.4*	56.1	12.5	19.1	21.1	23.1
				Observations					
Ground based			79.9				-		

Table 4.2. Simulations with hexagonal plates and spheres again produced the highest liquid water path and dendrites the lowest for a given IN concentration. As in the single layer case, small and fast falling plates and spheres produced the greatest liquid water path compared to large and slow falling plates and spheres. The other two combinations (large, fast falling and small, slow falling) produced results very close to each other. The large dendrites are again associated with very low liquid water path and the small dendrites with a higher liquid water path and high sensitivity to IN concentration. The terminal fall speed has only a small impact on simulated water paths for dendrites.

Similar to the single layer case, one simulation for each habit was selected

to compare against ground-based liquid water retrievals (Turner et al., 2007) and airborne measurements (data from DOE-ARM archive). Time series of predicted and retrieved liquid water paths and predicted ice water path are shown on Figure 4.7a and 4.7b. No clouds were produced by any simulation for the first 10 hours. The simulation with dendrites overestimated peaks in the liquid water path in the first and last 24 hours and underestimated it in the middle of the simulation. The experiment with spheres provided a better match to the retrieved LWP, but underestimates LWP for most of the simulation, except for the last 24 hours. The best correspondence with observations was achieved in the case of hexagonal plates with the simulated LWP following observations reasonably well. Unfortunately, no ice water path data are available. However, a comparison with Figure 9 in Morrison et al. (2008b) reveals that our values were on average two times lower than the retrieved IWP. Liquid and ice water vertical profiles observed during the Oct 6 flight (DOE-ARM data archive) and simulated profiles, averaged for the duration of the flight, are presented on Figure 4.8a and 4.8b. Both aircraft (Fig. 4.8a) and radar observations (Rambukange and Verlinde, personal communication) indicate the presence of four to five liquid layers. At the time of the observations the simulation with spheres produced only one liquid layer at height of about 1000 m and completely missed the layers above. Two layers were detected in the case with hexagonal plates – one around 1000 m and one at about 3000 m. The LWC of both layers is overestimated. In addition to these two layers, the simulation with dendrites produced a third layer at a height of about 2000 m. In this case, it appears that observed layers at 3250 m and

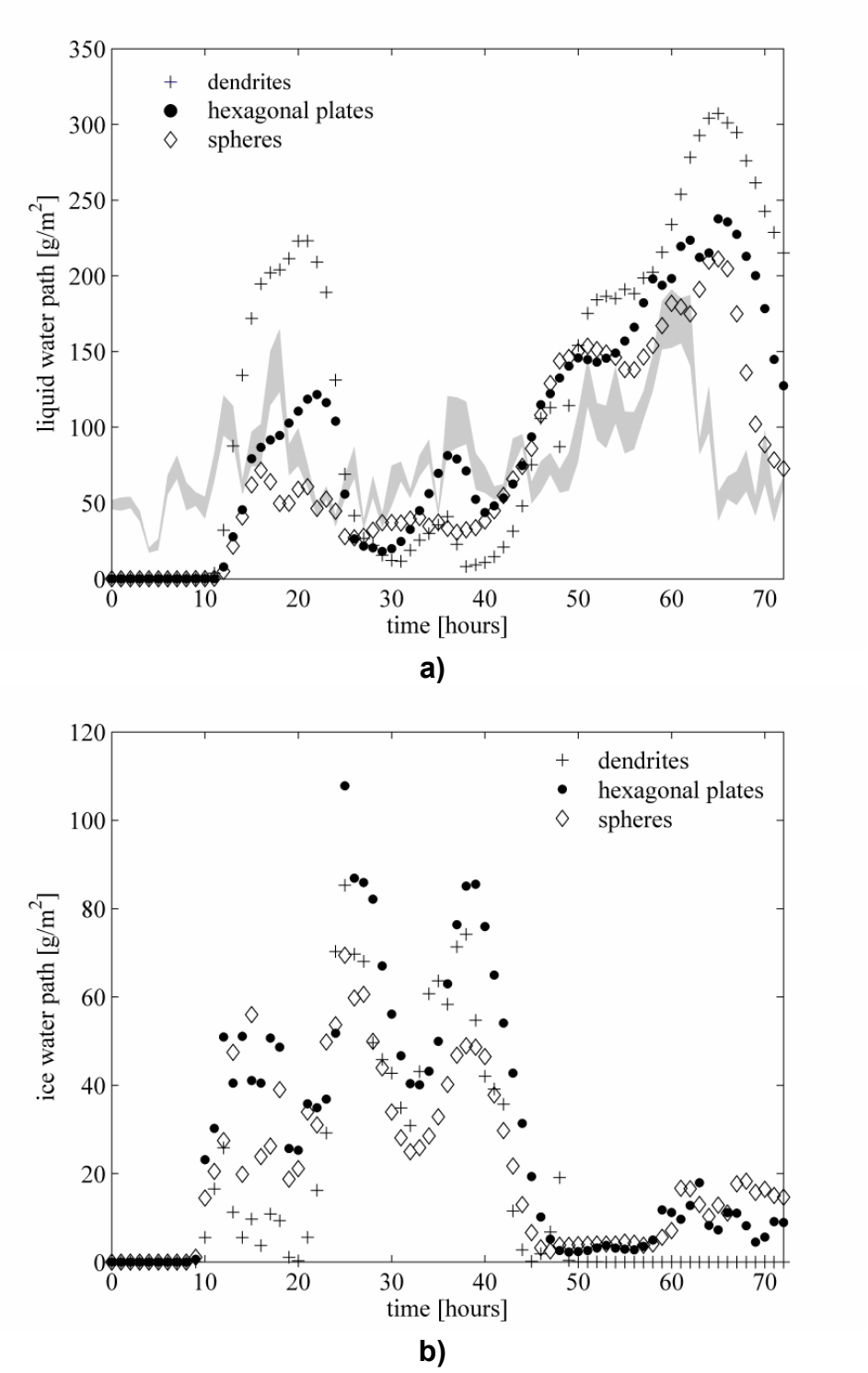

Figure 4.7: Time series of simulated (symbols) and retrieved (shaded) **(a)** liquid and **(b)** ice water path [gm^{-2}]: multi-layered clouds case. Simulated quantities are domain averaged. Shaded area in **(a)** represents 95% confidence interval of observational data.

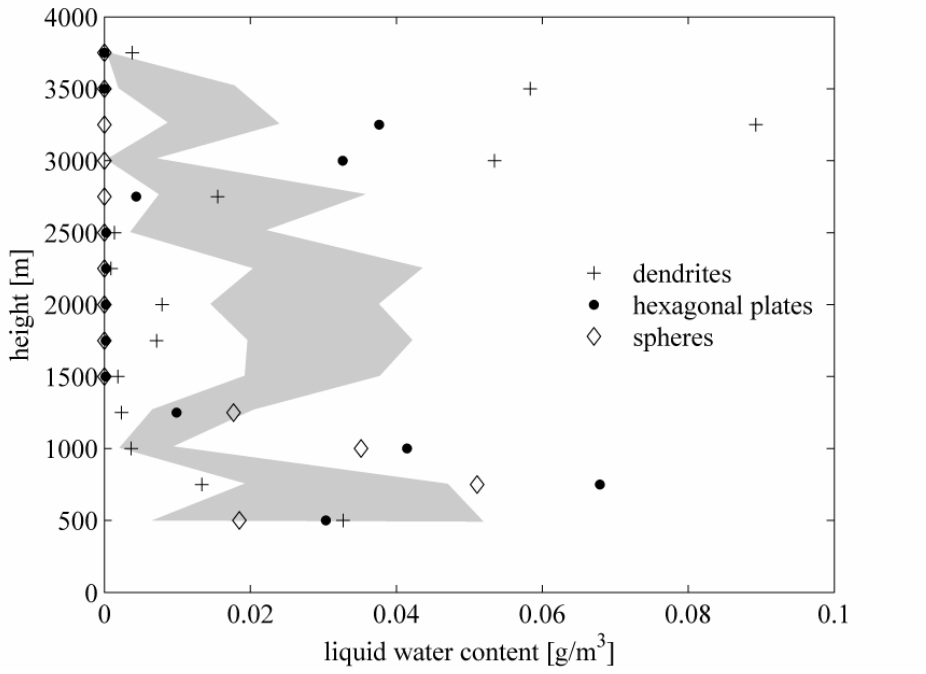

a)

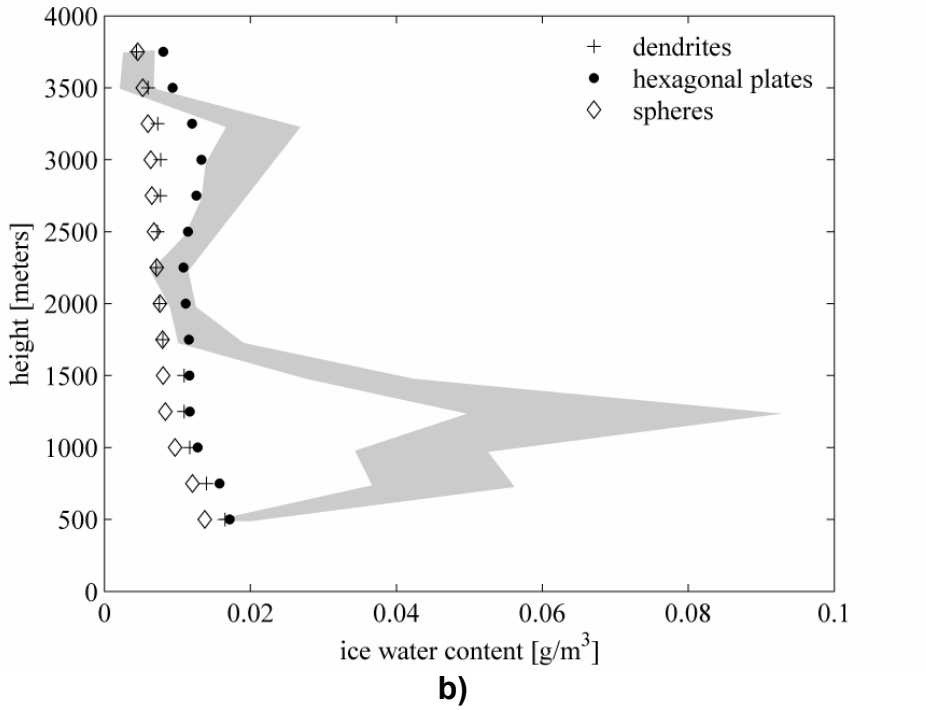

b)

Figure 4.8: Time-averaged vertical profiles of **(a)** simulated domain averaged (symbols) and observed (shaded) liquid and **(b)** ice water content [gm^{-3}]: multi-layered clouds case. Simulated and observed quantities are averaged over the flight duration. Shaded area represents 95% confidence interval of observational data.

2750 m (Fig. 8a) are combined into one layer in the simulation. The same could be argued about layers at 2250 m and 1750 m. The vertical grid spacing at this height is about 90-100m, which is at the limit of the models' ability to resolve the layers. The liquid water content of the top layer is significantly overestimated, however. All three simulations underestimate the ice water content, especially in the lower half of the cloud system – between 1500 m and 500 m. Above 1500 m, the simulation with hexagonal plates provides a reasonable match to the observations.

The different layer structure in these simulations begs the question – Is crystal habit related in some way to liquid layer formation, layer splitting and dissipation mechanisms? Answering this question completely is beyond the scope of this study, but it is helpful to look at the differences in the cloud vertical structure produced by the different simulations. Figure 4.9 shows simulation averaged liquid water profiles for the three crystal habits at relative IN concentrations of one and 50. The number of liquid layers in these simulations varies from one (dendrites at N_{IN}=50) to five (spheres at N_{IN}=1). At relative IN concentration of one, the "highest LWP" simulation with dendrites (Figure 4.9a) produces three layers, as does the simulation with hexagonal plates (Figure 4.9b), but with slightly higher liquid water content (bottom layer) and thickness (top layer). In addition to these three layers, the "highest LWP" simulation with spheres has two additional layers – one above 4000m and one below 1000 m (Figure 4.9c). Increasing the relative IN concentration to 50 decreases the number of layers for both "highest LWP" dendrites and hexagonal plates. The

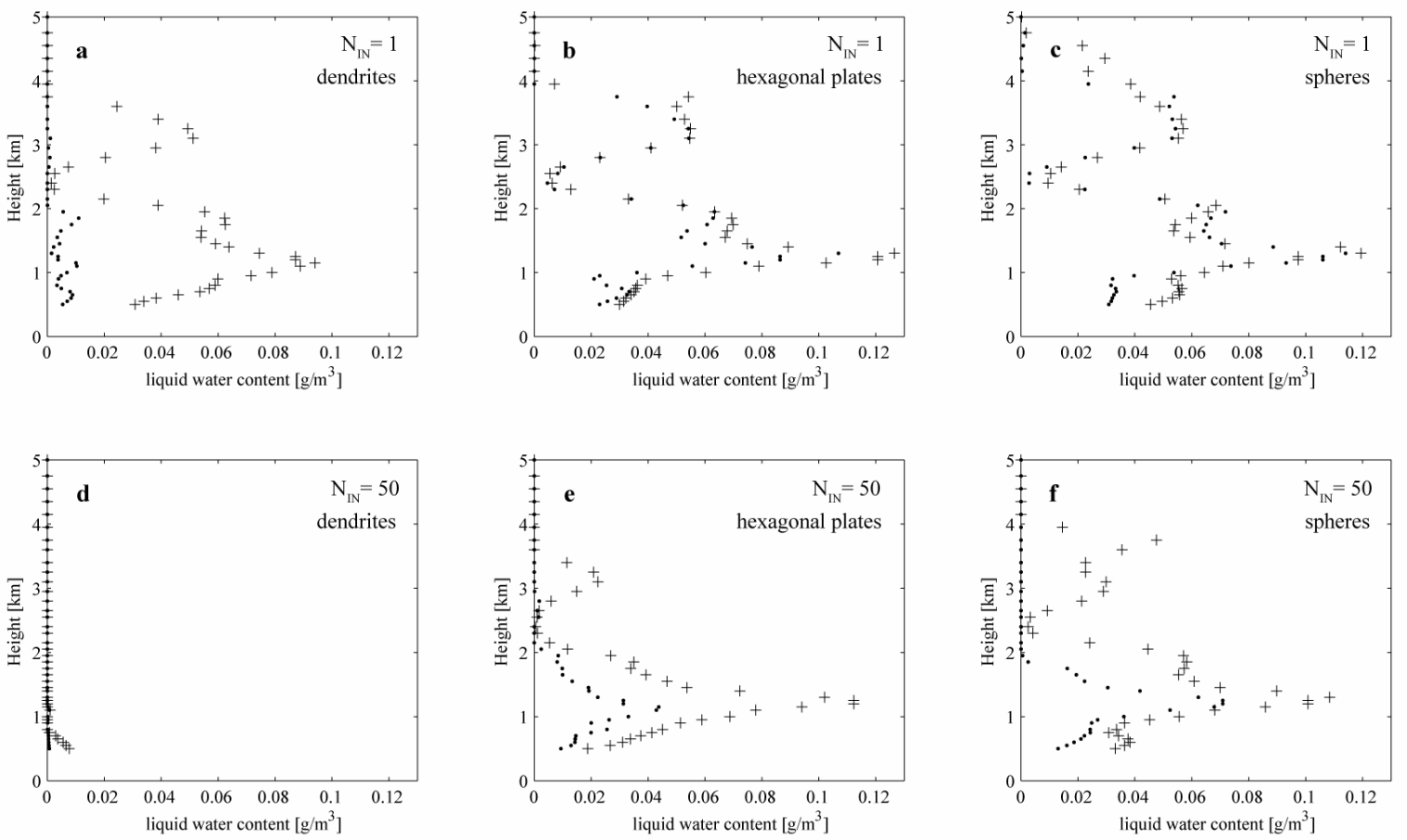

Figure 4.9: Simulation and domain averaged vertical profiles of liquid water content [gm^{-3}] for different habits at relative IN concentration of one **(a)**, **(b)**, **(c)** and 50 **(d)**, **(e)**, **(f)**. Crosses denote simulation producing highest liquid water path, and dots denote simulation producing lowest liquid water path.

most drastic is the difference in “lowest LWP” spheres – from five layers to one (compare Figure 4.9c and 4.9f). However, depleting the liquid does not necessarily always lead to decrease in number of liquid layers. Compare “highest LWP” spheres on Figure 4.9c and 4.9f. At N_{IN}=50 the top layer has disappeared, however, the thick layer between 2500 and 4000 on Figure 4.9c has split into two layers on Figure 4.9f, thus keeping five layers. Similar splitting, caused by liquid depletion, is observed on Figure 4.9a and Figure 4.9b (“highest LWP” to “lowest LWP” transition) below 1000 m.

4.4 Discussion

In the previous section we presented results of simulations of single and multi-layered mixed-phase clouds. Both cloud systems showed a similar response to sensitivities using different ice crystal habits. Despite all of the similarities between the results of the two cases, there are also some interesting differences. Unlike the single layer case, in the multi-layered case, simulations using small and fast spheres produced a higher liquid water path than that of small and fast falling plates. This could be explained by the larger vertical extent of the cloud system in this case and the larger fall velocity of spheres. As discussed above, the liquid water depletion by the growing ice crystals is proportional to their depositional mass growth rate and in-cloud residence time. With so chosen mass-dimensional and terminal fall velocity relations, small spheres exhibit faster growth and spend less time inside the cloud layer than the small plates. In the single layer case, the faster growth of the small spheres is

more important than the greater in-cloud residence time of small plates and leads to greater liquid water depletion. In the multi-layered case, because of the larger vertical extent of the liquid layers, the situation is reversed and the liquid water path of the small spheres is higher (Fig. 4.6a).

The other difference between the two cases is related to the lack of sensitivity to mass-dimensional and terminal fall velocity relations at low IN concentrations in the single layer case for spheres and plates. In the multi-layered case, however, even at low IN concentration the individual series of simulations are well separated. In the single layer case, the strong cloud top inversion effectively isolates the boundary layer and the initial IN in the cloud layer are depleted very quickly by nucleation-scavenging. Consequent IN activation is then possible only through supersaturation increase or entrainment of IN-rich air from above the cloud layer. Both processes are not well resolved at the grid spacing used here and as a result, the ice crystal concentration and consequently, liquid water consumption by the ice crystals is very low. In the multi-layered case IN activation occurs over several layers up to a 5 km height, so the IN are not exhausted and liquid water uptake by the ice crystals remains significant. In addition, the seeder-feeder mechanism is probably very important here as well. Taken together, along with the very thin nature of the layers, the model results suggest that the multi-layered case should have a different response at low relative IN concentrations.

In simulations of both single and multi-layered cases, the use of dendritic shapes led to a very high sensitivity of simulated cloud fields to IN concentration,

in contrast to experiments with hexagonal plates and spheres. We performed another series of simulations with dendrites to determine the parameters (mass-dimensional, terminal fall velocity relations and shape factor) responsible for this behavior. Since results from both cases were similar, the additional experiments were performed only on the single layer case.

In the first set of simulations the mass-dimensional relation was replaced with that of small hexagonal plates (Fig. 4.2a). Results from this set of simulations together with "standard" simulations (where mass-dimensional relations appropriate for dendrites are used) are illustrated in Figure 4.10. At low relative IN concentrations the LWP in new simulations increased up to the values of simulations with hexagonal plates and spheres, but the LWP quickly drops down as the IN concentration is increased. IN sensitivity is lower than that of the original dendrite simulation but still sufficiently higher than that of simulations with hexagonal plates and spheres. Figure 4.10 also illustrates an interesting effect. For all three mass-dimensional relations simulations with fast-falling crystals produce lower liquid water path than the simulations with slow-falling crystals. An analysis of these simulations suggested that this was caused by enhanced ice crystal growth due to the ventilation effect. Whether ventilation causes LWP to decrease depends on how much it increases growth in comparison to how quickly the increased fall-speed can remove crystals from the cloud. As the terminal fall-speed is increased further, the residence-time influence of the fall-speed becomes more important than the ventilation effect and so LWP increases.

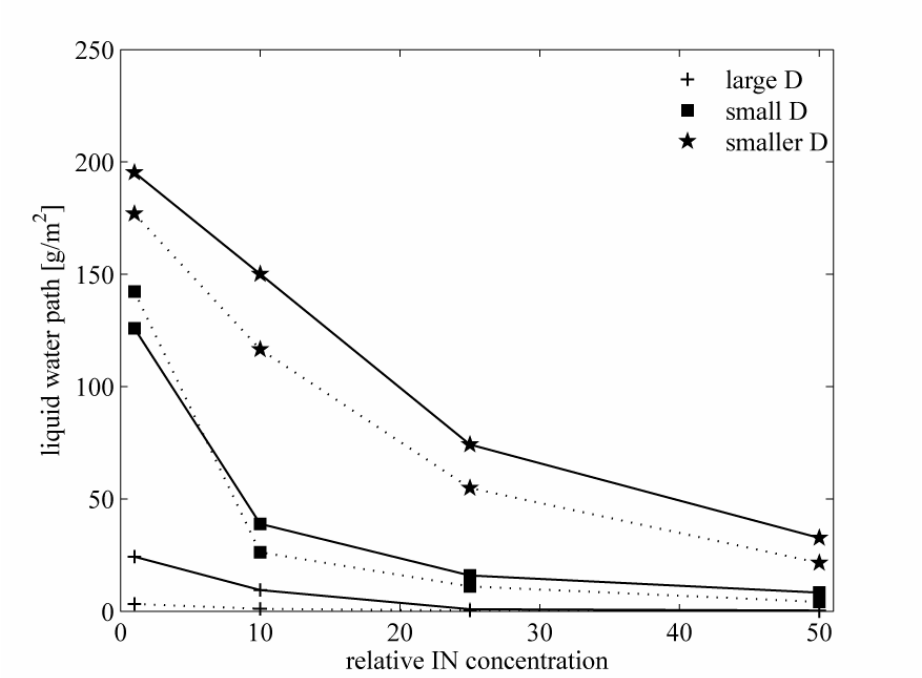

Figure 4.10: Domain and simulation averaged liquid water path for simulations with slow (solid line) and fast (dotted line) falling dendrites as a function of IN concentration. IN concentration is relative to 0.15L^{-1}.

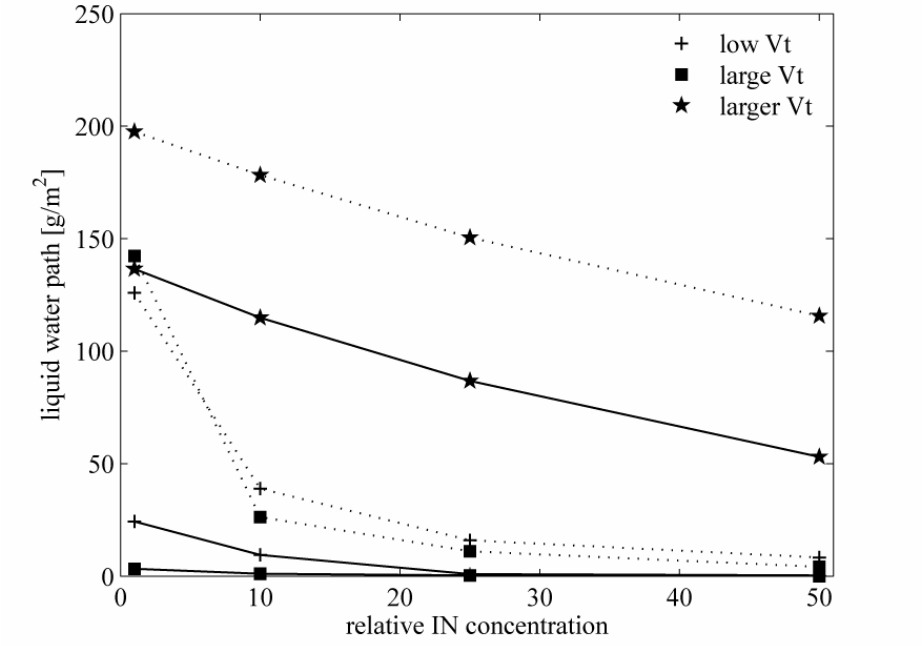

Figure 4.11: Domain and simulation averaged liquid water path for simulations with large (solid line) and small (dotted line) dendrites as a function of IN concentration. IN concentration is relative to 0.15L^{-1}.

In the next set of simulations we used fall velocity relation for fast falling hexagonal plates (Fig. 4.2b) and mass-dimensional relations appropriate for dendrites. This has the effect of removing dendrites more quickly from the cloud. In the previous simulations with dendrites we showed that their sensitivity to the fall velocity relation is minimal. However, this is not the case when the fall velocity is increased beyond the limits appropriate for dendrites (Figure 4.11). The liquid water path of large dendrites increased significantly compared to the original dendrite simulations and LWP of small dendrites is inside the range typical for hexagonal plates (c.f. Fig. 4.5a). It should be emphasized, though, that these “composite” habit tests are not physical. They are a method to illustrate the relative importance of the physical factors controlling liquid water depletion. Our results show that while terminal fall speeds are certainly important for removing ice from the cloud layer, and hence increasing the cloud lifetime, they can not be considered alone. In other words, one cannot disregard the other parameters used to describe the habit of the ice crystals.

As it was discussed above, the shape parameter of dendritic crystals varies depending on the arms aspect ratio (Westbrook et al., 2008). To account for this variability, we included a series of runs where the shape parameter was varied from the baseline value of 0.31 down to 0.22. This covers the realistic range of S for dendrites, c.f. Sheridan, 2008). Results from this series are shown on Figure 4.12. For the large dendrites changes in the shape factor have a small impact on results of the simulations. Large dendrites grow very fast and deplete all the liquid water regardless of the value of S. For the small dendrites, however,

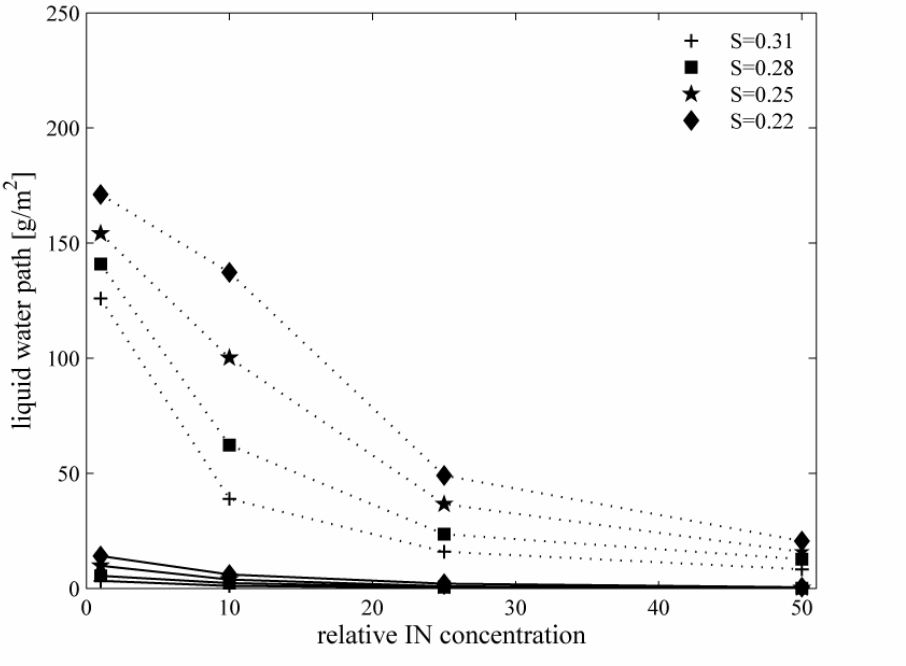

Figure 4.12: Domain and simulation averaged liquid water path for simulations with large (solid line) and small (dotted line) dendrites as a function of IN concentration. IN concentration is relative to $0.15L^{-1}$.

the impact is significant. Although the sensitivity to IN concentration still remains high, decreasing the shape parameter value leads to a considerable increase in the LWP.

This result is as important as our previous two experiments where both mass-dimensional and fall velocity relations were varied. The results show significant sensitivity to a parameter that defines dendritic habit influences on growth. Though our, and most other, models fix the value of S for a particular habit, in reality, as crystals grow their aspect ratios change which then causes S to change (Chen and Lamb, 1994). This feedback between evolving habits and vapor growth is not captured by our model nor by most other simulations of

mixed-phase clouds (Harrington et al., 1999; Fridlind et al., 2007; Morrison et al., 2008a) but it turns out to be important (Sheridan, 2008). Our results suggest that improving shape prediction in mixed-phase cloud model is quite important.

4.5 Summary

In this chapter we used high resolution two-dimensional cloud-resolving model to examine the influence of the assumed ice crystal habit on simulated cloud liquid and water content and their sensitivity to IN concentration. Three basic crystal shapes were used in these simulations – hexagonal plates, dendrites and spheres. For each crystal shape we performed series of simulations using various combinations of the upper and lower limits of the mass-dimensional and fall velocity relations. By combining the extremes in the mass and fall-speed relations our simulations span the range of mixed-phase cloud sensitivity to the way crystal habit is parameterized in a bulk microphysical model.

We presented results of simulations of two different cases – single and multi-layered mixed-phase clouds. Both cloud systems showed similar response to sensitivity experiments using different ice crystal habits. Simulations using hexagonal plates and spheres produced the largest liquid and smallest ice water path. Their sensitivity to IN concentration is rather low. Simulations with dendrites showed greater ice water path and smaller liquid water path, and much stronger IN sensitivity, very similar to our results in Chapter 3. The strong sensitivity to IN concentration and crystal size suggests that in the case of dendrites the balance

between liquid water production and consumption is very delicate. Small changes in crystal size or concentration immediately lead to dramatic changes in simulated cloud fields. This is probably the reason for the strong sensitivity of modeled LWP and cloud longevity to IN shown by Harrington (1997), Harrington and Olsson (2001a), Jiang et al. (2000), Prenni et al. (2007) as compared to the weaker sensitivity shown by Morrison et al. (2008a) and Fridlind et al. (2007). The former simulations assumed dendritic crystals whereas the latter simulations assume essentially spherical particles.

Our results show that the range of predicted LWP and IWP in a model appears to depend greatly on the choice of mass-dimensional and fall-velocity relations. However, our simulations also show that almost any range of LWP and IWP can be produced by judicious choice of mass and terminal fall speed relations. Furthermore, precisely because of the large potential range of LWP and IWP, it appears that simulating changes in crystal habit is of vital importance for simulations of mixed-phase clouds.

Chapter 5

Influence of ice nucleation mechanisms on simulated mixed-phase cloud structure

In the previous chapters we concentrated mainly on the liquid and ice water content partitioning in simulated mixed-phase clouds. A common problem with all simulations presented in those chapters is that the simulations fail to reproduce observed ice crystal concentrations. This problem is common for modeling studies of heterogeneous ice formation in mixed-phase clouds and stems from the fact that measured IN concentrations (and consequently ice formation in models) are often several orders of magnitude lower than measured ice crystal concentrations (Mossop, 1970, 1985). This discrepancy has not been resolved to date (e.g. Cantrell and Heymsfield, 2005), though a number of possible nucleation mechanisms have been suggested.

Recently, Fridlind et al. (2007) examined a variety of ice nucleation mechanisms and showed that two of them – IN formation from drop evaporation residuals ("evaporation IN", Rosinski and Morgan, 1991) and drop freezing during evaporation ("evaporation freezing", Cotton and Field, 2002), could account for the observed ice crystal concentrations and mass in Arctic mixed-phase clouds while retaining sufficient liquid water. Recall from Chapter 2 that evaporation IN nucleation occurs in the following manner. It is postulated that a small fraction of all evaporating drops release an IN to the environment. In contrast, evaporation freezing is postulated to occur through the freezing of a small fraction of evaporating drops.

While the above two nucleation mechanisms are capable of producing liquid and ice water paths and ice crystal concentrations similar to observations, it must be kept in mind that these are typically first-order features of the simulated cloud fields. Moreover, as Fridlind et al. (2007) showed, it is not possible to distinguish between evaporation IN and evaporation freezing in the M-PACE cases. Each postulated nucleation mechanism produces similar results. Hence, comparisons of concentrations along with LWP and IWP are somewhat insufficient to distinguish amongst the nucleation mechanisms. In this section, we explore whether ice nucleation mechanisms have a detectable impact on mixed-phase cloud structure. If so, then it could be possible to distinguish nucleation modes based on observed cloud structure. For instance, given that both postulated nucleation mechanisms are linked to drop evaporation, it could be the case that ice formation is strongly linked to cloud-scale downdrafts.

5.1 Simulation design

In this chapter we focus again on the single-layered mixed-phase cloud, or period B from M-PACE - the period from 17 Z on October 9 to 5 Z on October 10, 2004. We do this for a number of reasons. First, it is the same case as simulated by Fridlind et al. (2007) allowing direct comparisons with their results. Second, the single-layered case is the most extensively studied to date because it is the simplest.

Both postulated nucleation mechanisms (“evaporation freezing” and “evaporation IN”) require the resolution of cloud-scale motions. Both require the

explicit evaporation of water droplets in downdrafts which cannot be captured in a cloud-resolving model since the grid-spacing is too coarse. Instead, we employ an eddy resolving model (ERM), which is the two-dimensional counterpart to three-dimensional large eddy simulation. The computational domain has 168 horizontal grid points with 60 m spacing and 100 vertical grid points with 30 m spacing in the lower 1800 m, stretching to 200 m at domain top. Cyclic boundary conditions are applied on the lateral boundaries. The model is initialized with a prescribed sounding and constant winds. The large scale forcing and surface fluxes, developed specifically for case B of M-PACE model inter-comparison study (Klein et al., 2008) and used in Chapter 4, are also used here. The soil-vegetation and sea-ice submodels of RAMS were not used in this study and the lower boundary is assumed to be ocean surface. The duration of the simulation is 12 hours, with a 1 second time-step.

For simulations presented in this chapter, three new nucleation mechanisms were included in the model: “evaporation freezing”, “evaporation IN” and immersion-freezing (see Chapter 2). The ice nucleation rate due to immersion-freezing is parameterized following Reisin et al. (1996) which is essentially the formulation from Bigg (1953) and is computed using Eq. 2.4. The “evaporation freezing” mechanism is parameterized by transferring number concentration and mass mixing ratio of a fraction of evaporating cloud droplets to pristine ice category similarly to Fridlind et al. (2007). Simulations where one in 10^5-10^6 evaporating droplets freeze provides a reasonable match to observations. The parameterization of “evaporation IN” is complicated by the fact

that the IN so produced must be stored. Following Rosinski and Morgan (1991), we assume that one in 10^5-10^6 evaporating droplets creates an IN which are allowed to act only in deposition/condensation-freezing mode. If the local supersaturation allows for additional IN activation they are activated immediately. If they are not immediately activated, the IN are stored in an scalar array and transported by in-cloud circulations.

5.2 Results

To examine the influence that the different ice nucleation mechanisms might exert on the structure of the simulated clouds we ran four simulations; one for each of the ice nucleation mechanisms we consider – deposition/condensation-freezing, “evaporation IN”, “evaporation freezing” and immersion-freezing. Deposition/condensation-freezing mechanism was always active and the other three mechanisms were used separately.

In order to illustrate the impact that nucleation mechanism has on cloud structure, we begin by examining the “evaporation IN” simulation. This simulation (Figure 5.1) produced a cloud structure consistent with radar and airborne observations. Simulated liquid and ice water content show very good agreement with the observed vertical profiles (compare with Figure 4.4). Consistent with radar retrievals (Seroka, 2008; Verlinde personal communication), the simulated updrafts contain most of the cloud ice mass. Conversely, downdrafts contain less ice and are associated with excursions of the liquid water content to lower

altitudes than is the case with updrafts. These results also match observations (Verlinde, personal communication).

Observed and modeled vertical profiles of ice crystal concentration are presented in Figure 5.2. When only the deposition/condensation-freezing nucleation mechanism is active, simulated ice crystal concentrations are one to

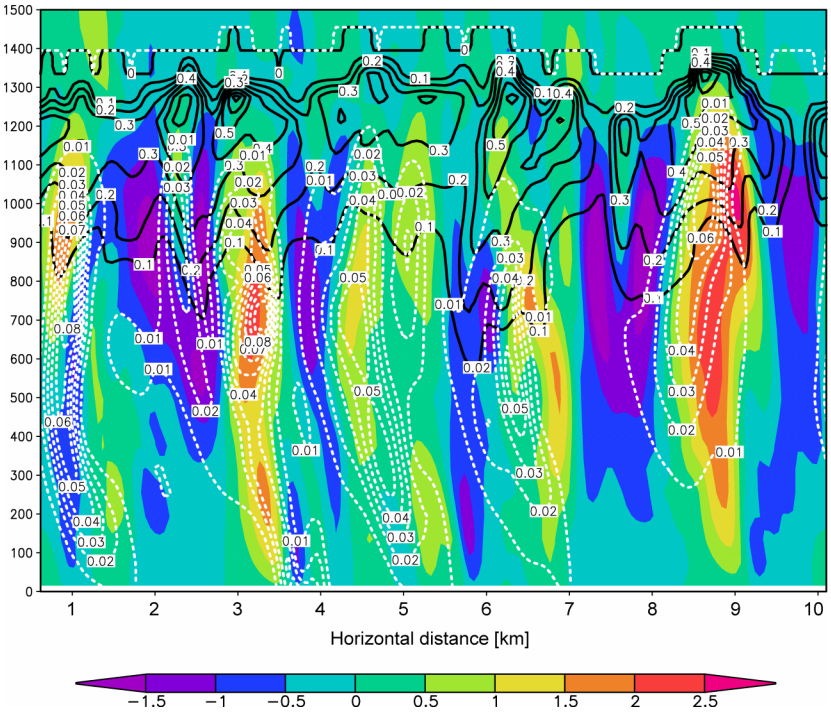

Figure 5.1: Simulated vertical velocity [m/s] (color shaded), liquid water content [gm^{-3}] (black solid contours) and ice water content [gm^{-3}] (white broken contours) at t = 120 min for "evaporation IN" simulation

two orders of magnitude lower than the observed concentrations (Figure 5.2a and b), similar to the results discussed in Chapter 4 and by Fridlind et al. (2007). When either evaporation IN or immersion-freezing mechanisms is included in the simulation, the ice crystal concentrations increase significantly, reaching values in excess of 1 L^{-1}, providing much better agreement with the observational data

(Figure 5.2a, c and d). Ice crystal concentrations in the “evaporation freezing” simulation are very close to those of the “evaporation IN” simulation and so are not shown.

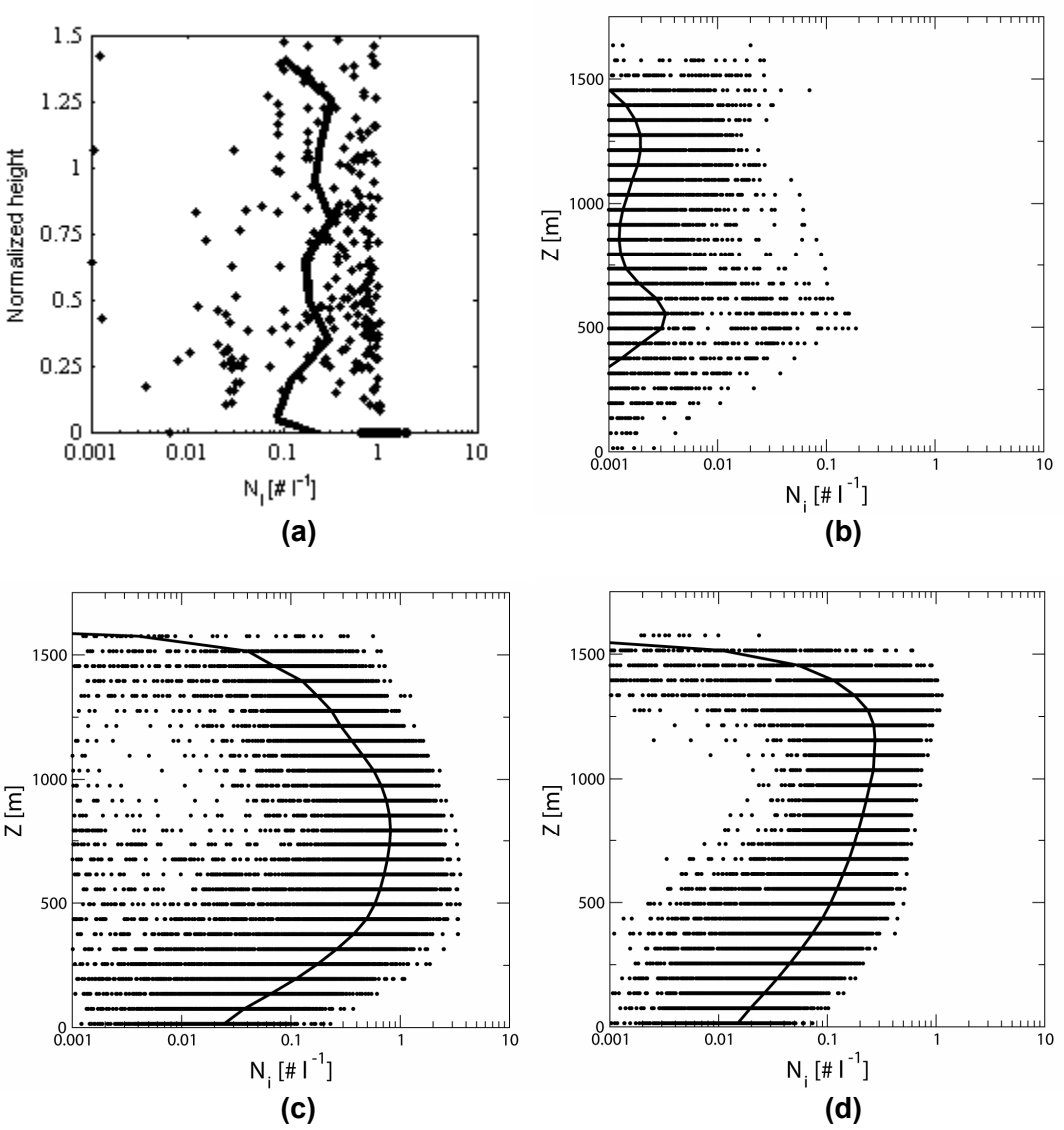

Figure 5.2: Vertical profiles of ice crystal concentrations: **(a)** observations; **(b)** deposition/condensation-freezing nucleation, **(c)** “evaporation IN” and **(d)** immersion-freezing

Taking into account that in the “evaporation freezing” simulation we instantaneously freeze approximately the same number of evaporating droplets

as we form IN in the “evaporation IN” run, this result should not be surprising. Our results are similar to those of Fridlind et al. (2007), which gives us some confidence in the fidelity of our simulations. However, it is difficult to distinguish between the evaporation freezing, evaporation IN, and immersion-freezing nucleation mechanisms based on concentration and water paths alone.

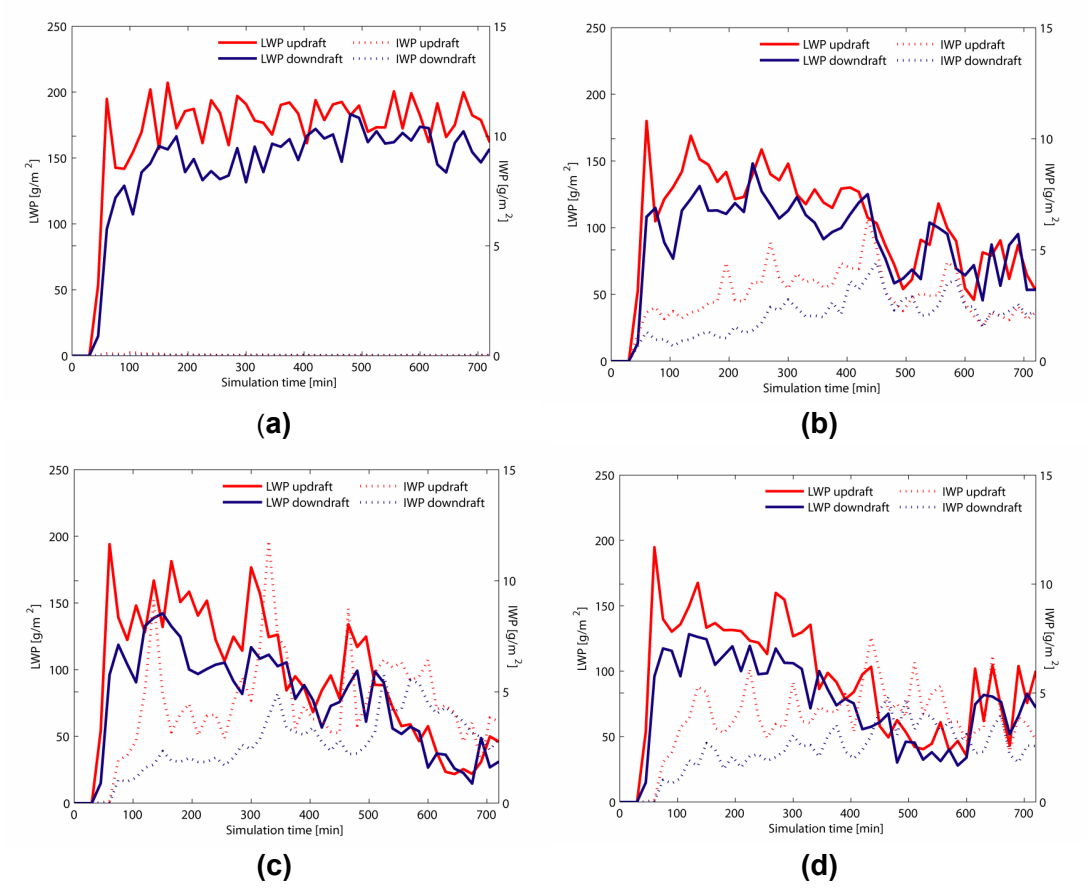

Figure 5.3: Liquid (solid line) and ice (broken line) water path [gm^{-2}] in updrafts (red) and downdrafts (blue) for **(a)** deposition/condensation-freezing nucleation; **(b)** immersion-freezing; **(c)** “evaporation IN” and **(d)** “evaporation freezing”

To illustrate cloud structure with time, the liquid and ice water paths for all

simulations are presented in Figure 5.3. The deposition/condensation-freezing run produces liquid water paths that are too high as compared to observations and negligible ice water path. The very low ice water path is consistent with the very low ice concentrations (Figure 5.2b). Liquid and ice water paths in the simulations with the other nucleation mechanisms compare reasonably well with observations (~120 g m^{-2} and ~8-30 g m^{-2}, for liquid and ice water path, respectively). In all four runs the simulated ice water path is higher in the updraft regions of the cloud for most of the simulation period, which is also consistent with radar observations. The same holds true for the liquid water path. However it should be noted that deposition/condensation-freezing produces higher ice water paths in updrafts only during the very early stages of the simulations (first 200 min.). For the remainder of the deposition/condensation-freezing simulations, the ice water paths are roughly similar between the updrafts and downdrafts, a distinct difference as compared to the other nucleation mechanisms. How do these general features match the observed structure of mixed-phase clouds?

Simulated cloud structures are compared to the observations in Figure 5.4 and Figure 5.5. Radar observations (top row in both figures) show an interesting separation of the ice water content in the cloud. At cloud top the ice water content is highest in the strongest updrafts. As the height decreases, however, the maximum in the ice water content shifts towards lower velocity. At the cloud base, the highest ice water content is observed in the strongest downdrafts. The

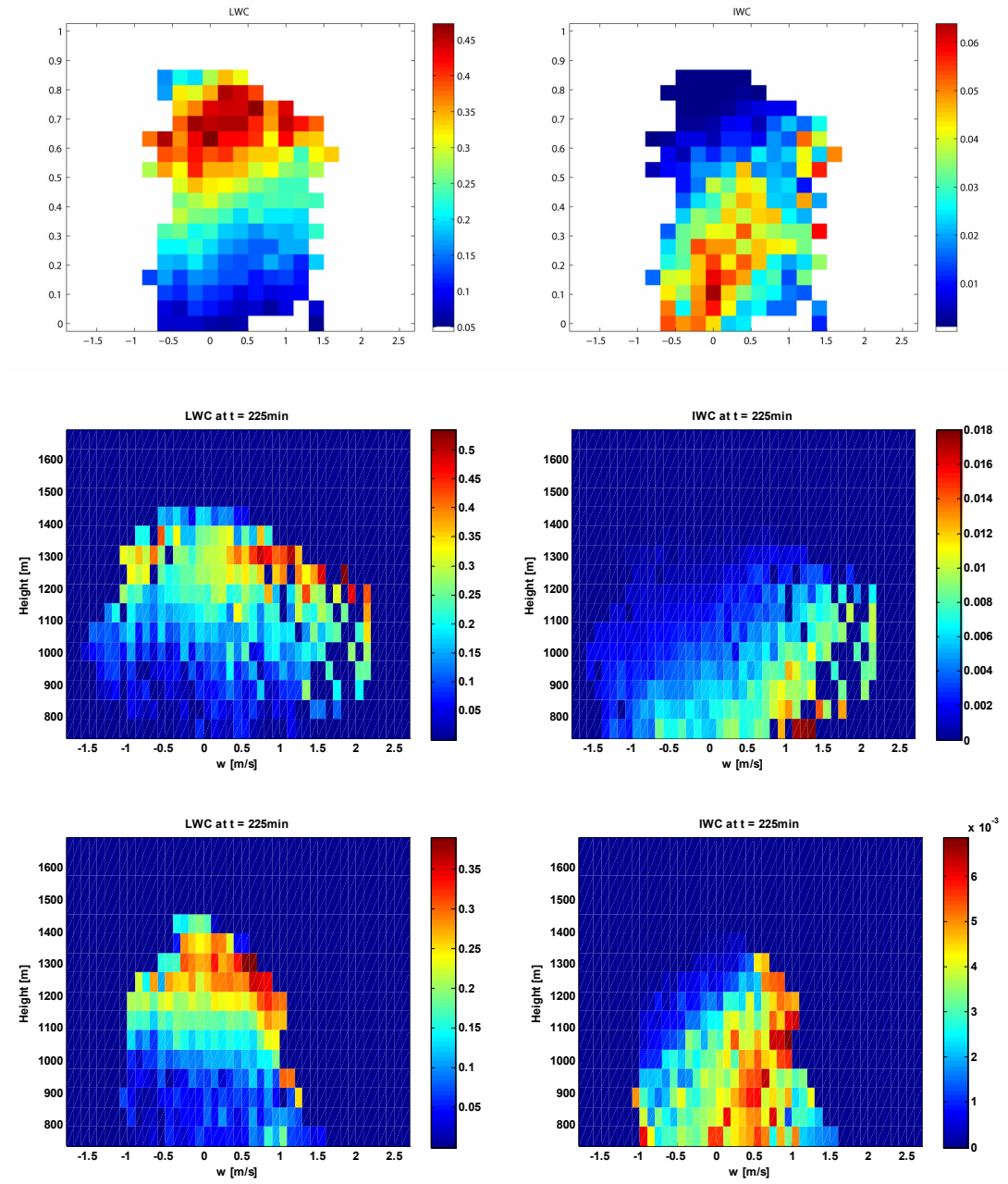

Figure 5.4: Retrieved and modeled liquid (left) and ice (right) water content [gm^{-3}]: radar retrievals (top row), “evaporation IN” (middle row), immersion freezing (bottom row)

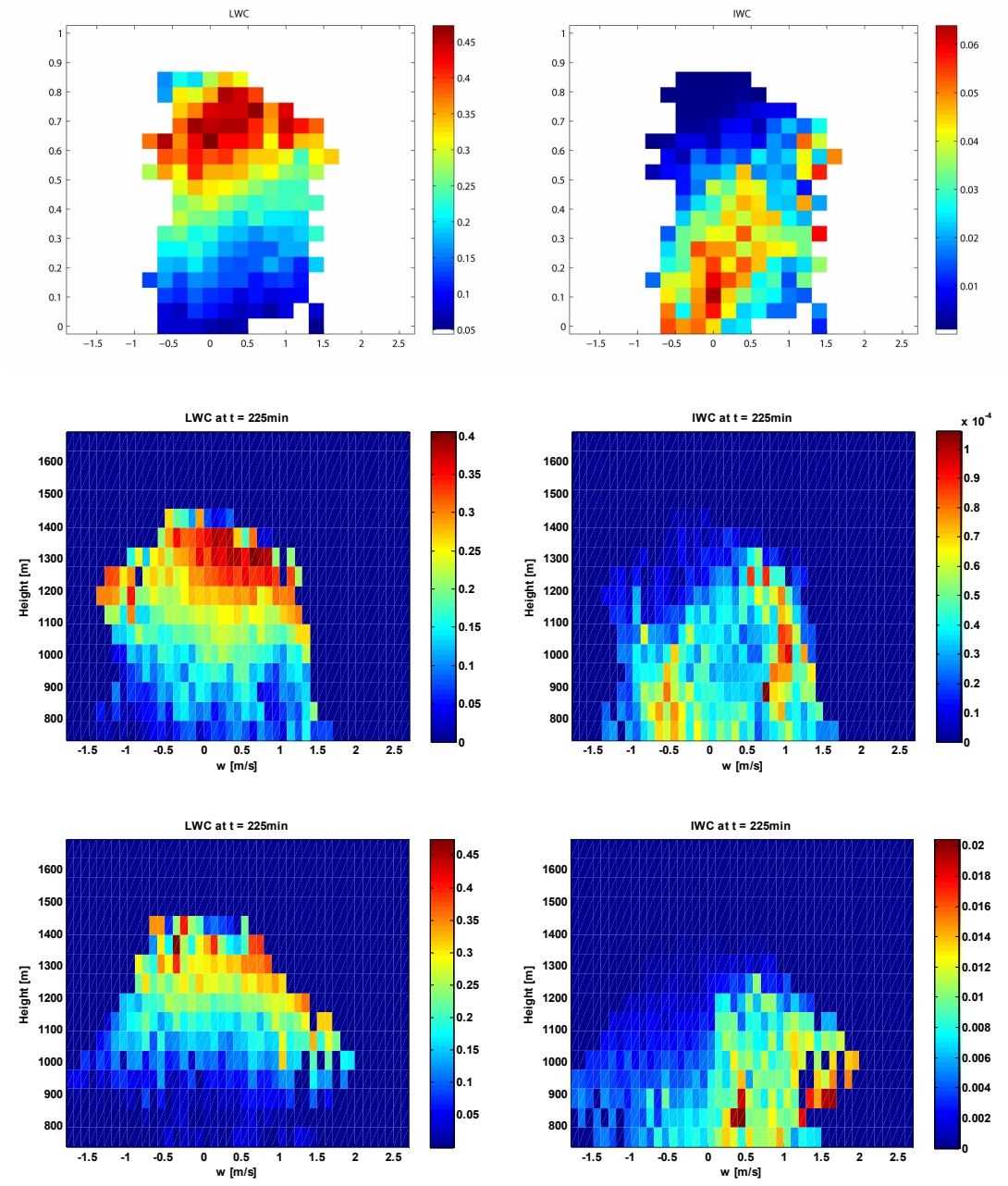

Figure 5.5: Retrieved and modeled liquid (left) and ice (right) water content [gm^{-3}]: radar retrievals (top row), deposition/condensation-freezing (middle row), "evaporation freezing" (bottom row)

liquid water content is highest at the top of the cloud and appears to be slightly correlated with positive vertical velocity (updrafts). All four nucleation mechanisms seem to be capable of reproducing this structure more or less successfully. The best agreement occurs with immersion-freezing (Figure 5.4, bottom row) and deposition/condensation-freezing (Figure 5.5, middle row) runs. However, keep in mind that these are snap-shots in time and that deposition/condensation freezing is able to maintain this structure for only the early part of the simulation, after which time the ice mass is equally partitioned between updrafts and downdrafts.

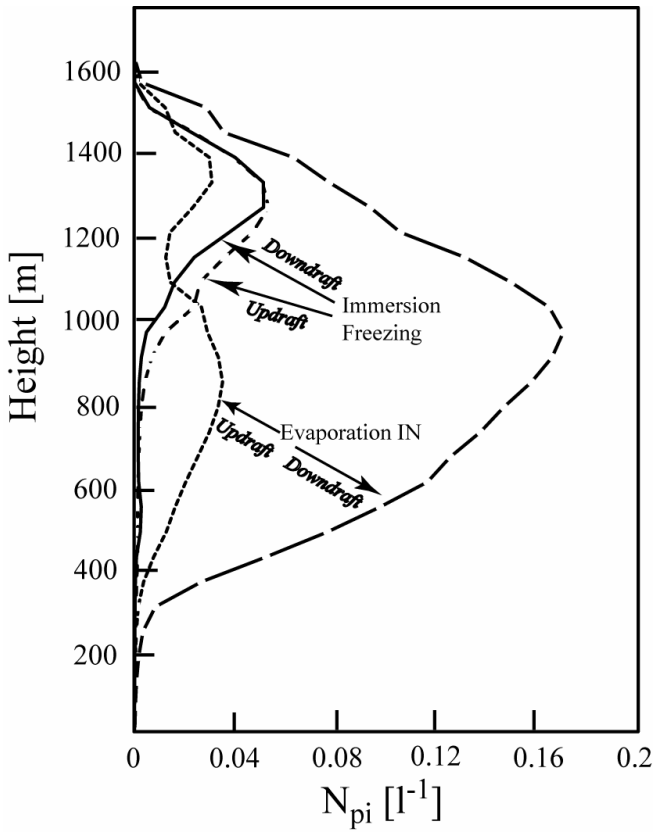

Figure 5.6: Vertical profiles of pristine ice concentration [L^{-1}] for “evaporation IN” and immersion-freezing runs

As a consequence, it seems that deposition/condensation is not able to maintain structures similar to those that are observed whereas the other three nucleation mechanisms can maintain such structures. The similarity in cloud structure produced by the different nucleation mechanisms poses another interesting question: if they all produce the same structure, how can we distinguish between them?

Figure 5.6 shows that each mechanism tends to produce the most small ice in different locations of the cloud even though the overall cloud structure is the same. Deposition/condensation freezing tends to produce ice everywhere throughout most of the simulation duration and is not shown. “Evaporation freezing” produces results similar to “evaporation IN” and is also not shown. In the immersion-freezing run the pristine ice is nucleated at the top of the cloud where the size of the cloud droplets is largest, temperatures are the lowest, and consequently the probability of freezing is greatest. In the “evaporation IN” run the ice crystals are nucleated predominantly in the downdrafts, where most cloud droplet evaporation occurs. These small crystals survive below liquid cloud base because this region is slightly supersaturated with respect to ice. The small crystals are then advected into the updrafts where they grow by vapor depositional growth. The fact that ice and liquid grow at the same time is not unusual (Korolev, 2007; Korolev and Field, 2008). This also explains why the largest pristine ice concentration is observed in downdrafts whereas the largest ice content (i.e. snow crystals) is in updrafts.

Consequently, the main difference between the nucleation mechanisms is the location in the cloud where the ice is initiated. In the case of “evaporation freezing” pristine ice crystals are formed immediately as cloud droplet evaporation takes place in the downdrafts and at cloud boundaries. In the “evaporation IN” case, although the IN are formed at the same locations as the ice in the “evaporation freezing” case, IN activation depend on the ice supersaturation. If the ice supersaturation is high enough to support the activation of all newly formed IN, then the “evaporation IN” mechanism becomes identical to “evaporation freezing”. If, however, not all newly formed IN are activated immediately after droplet evaporation non-activated IN are advected around by cloud updrafts and downdrafts until they reach a part of the cloud where conditions favorable for their activation exist. Thus, the “evaporation IN” mechanism could be thought of as having both a “local” (ice formed at the location where the IN are formed) and “non-local” component (ice formed elsewhere by advected IN). The above analysis would seem to suggest that “evaporation IN” forms ice locally, in the downdrafts. However, that is not completely correct.

Figure 5.7 shows a snap-shot of the liquid water content, ice concentration, and the unactivated IN concentration for the “evaporation IN” simulation. Note that a large concentration of IN exist immediately above cloud top. This large pool of IN is due to detrained air associated with updrafts. The evaporation of water droplets detrained above cloud top causes IN to be

released. These IN can then be entrained into the cloud layer at a later time, causing a rise in ice concentrations.

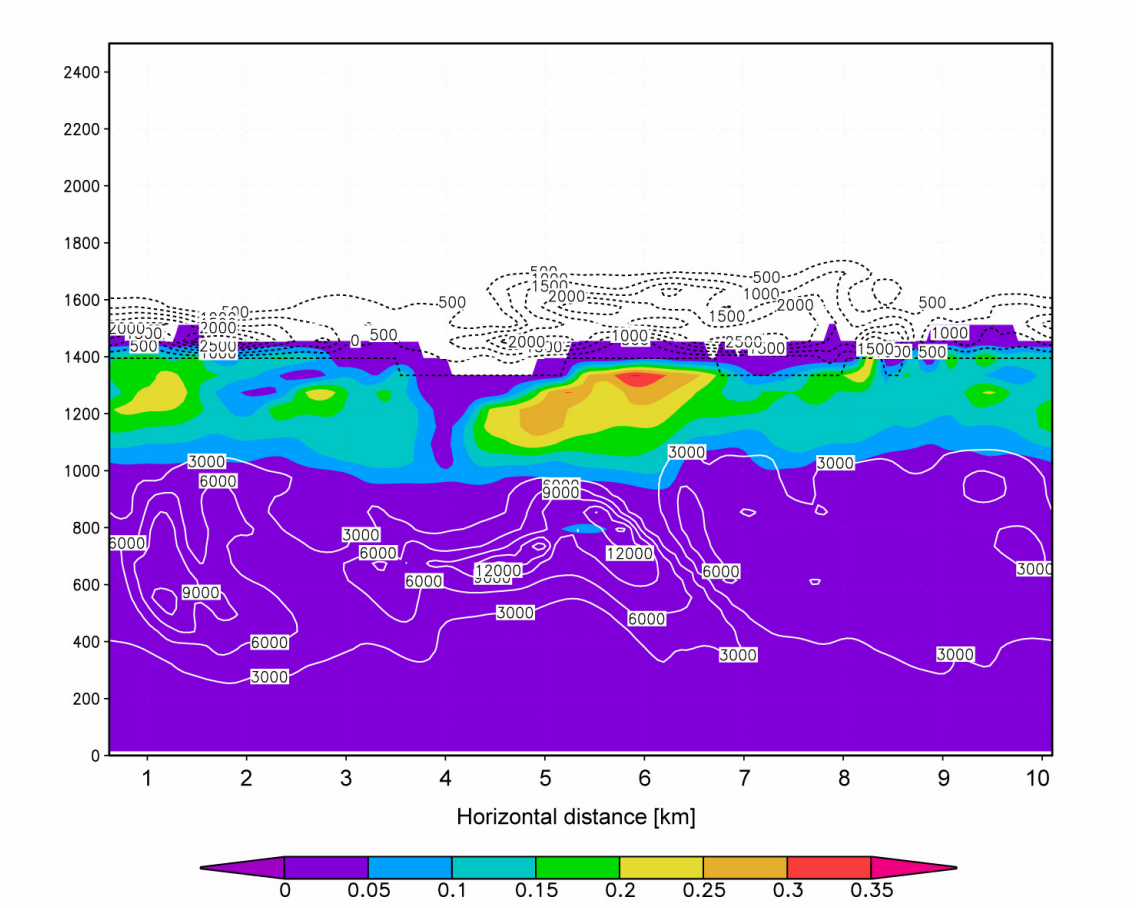

Figure 5.7: Liquid water content [gm^{-3}] (color shaded), ice crystal concentration [# m^{-3}] (white contours) and number concentration of unactivated evaporation IN (black, broken line contours)

This process is most certainly active in our simulated clouds, however more detailed analyses would have to be done to separate local and non-local IN nucleation in the “evaporation IN” simulations. The evidence at present is against this mechanism. If high IN concentrations were forming above cloud top due to detrained droplets, they surely would have been observed by the continuous-flow

diffusion chamber measurements of Prenni et al. (2007). However, no increases in IN concentrations were discerned above cloud top.

5.3 Summary

In this chapter we examined three postulated ice nucleation mechanisms with regard to their ability to 1) correctly simulate liquid and ice water content and ice concentrations in Arctic mixed-phase clouds; and 2) correctly reproduce the observed cloud structure. In contrast to deposition/condensation-freezing mechanism, all three of them were capable of producing ice crystal concentrations similar to the observed, while maintaining the liquid content of the cloud. Simulated liquid and ice water paths were also shown to match the observations. Deposition/condensation freezing cannot reproduce cloud structure correctly, except during the first ~ 200 min of the simulations. “Evaporation IN”, “evaporation freezing”, and immersion freezing could reproduce the observed cloud structure for extended periods of time. Distinguishing between the mechanisms poses a challenge, however.

An initial analysis shows that the location of ice formation may assist in distinguishing between the mechanisms. Immersion freezing produces ice at cloud top, deposition/condensation freezing produces ice everywhere, whereas “evaporation freezing” and “evaporation IN” tend to initiate ice in the downdrafts. “Evaporation IN” is complicated by the fact that it has both local and non-local effects. Ice can be formed locally at the same instant that the IN are formed, however the produced IN can also be advected. Our analysis shows that the

non-local effect could be important because IN pool above cloud top likely due to the detrainment of drops into the region above cloud top. These IN can then be entrained later causing ice formation.

Chapter 6

Summary and conclusions

Mixed-phase stratus clouds are the predominant cloud type in the Arctic during the winter and transition seasons and through various feedback mechanisms exert a strong influence on the Arctic climate. Because of the co-existence of ice and liquid water at sub-freezing temperatures, the correct representation of these clouds is a major challenge for any model. Various model intercomparison studies have shown that most climate and regional models tend to significantly underestimate the amount of liquid water in Arctic mixed-phase clouds, leading to systematic errors in the surface radiative budget. Results from previous studies of Arctic mixed-phase clouds suggest that inadequate parameterization of ice nucleation processes might be a possible reason for this discrepancy.

Using IN observational data collected during M-PACE we demonstrated that this is indeed the case. Our results show that the structure and the lifetime of simulated Arctic mixed-phase clouds are highly sensitive to the concentration of IN acting in deposition/condensation-freezing nucleation mode. The use of the IN parameterization derived from M-PACE measurements results in realistic simulations of mixed-phase cloud layers, very similar to those observed. In contrast, when higher IN concentrations, typical for mid-latitudes, are used in

simulations, the cloud layer rapidly glaciates, leading to errors in the modeled surface radiative energy budget of up to 90 Wm^{-2}. Although this result is not completely new, it is a first time such sensitivity has been demonstrated using a detailed mesoscale model.

We also examined the role of deposition/condensation-freezing, contact nucleation and the impact of IN transport by coastally-generated circulations. In our simulations, the contact nucleation mode could not produce significant ice water amounts unless the ambient contact IN concentrations were increased to unrealistically high values. Consequently, contact nucleation cannot be considered a significant source of continuous ice production in clouds at the temperatures simulated here. Instead, we found that local coastally-induced mesoscale circulations are responsible for maintaining the continuous ice precipitation along the coastline through transport of deposition/condensation-freezing IN from above the cloud layer. Therefore, the deposition/condensation-freezing nucleation is the dominant ice nucleation mode in our simulations. Our results also demonstrated that in order to correctly simulate Arctic mixed-phase stratus clouds models must correctly predict not only the number of heterogeneously nucleated ice crystals but also the cloud processing and removal of ice-nucleating aerosols through precipitation.

While all prior studies of Arctic mixed-phase clouds focus primarily on ice nucleation and ice concentrations, ice habit and how it is parameterized also affects the microphysical structure of simulated mixed-phase Arctic stratus. Liquid water evaporation by ice crystals depends not only on their concentration

but also on their in-cloud residence time and mass growth rate, both of which are related to ice crystal habit. Hence, liquid water depletion in mixed-phase clouds is controlled mainly by two factors: IN concentration and ice crystal habit. Consequently, simulated cloud sensitivity to IN concentration might depend on the assumed ice crystal habit.

To examine habit dependence we performed a series of simulations using a two- dimensional cloud-resolving model. We simulated two different cases from M-PACE - a single mixed-phase cloud layer and multiple liquid layers with ice crystals falling between them. Three basic crystal shapes were used in these simulations – hexagonal plates, spheres and dendrites. For each crystal shape we performed a series of simulations using various combinations of the upper and lower limits of the mass-dimensional and fall velocity relations reported in the literature. By combining the extremes in the mass and fall-speed relations, our simulations span the range of mixed-phase clouds sensitivity to the way crystal habit is parameterized in a bulk microphysical model.

Both cloud systems showed a similar response to the sensitivity tests. Simulations with hexagonal plates and spheres produced the largest LWP and the smallest IWP. The sensitivity to IN concentration in these simulations is rather low. Simulations with dendrites showed greater IWP and smaller LWP, and a much stronger IN sensitivity, which is very similar to the results of our mesoscale simulations. These tests also resolved a conflict between our simulations (e.g. Prenni et al., 2007) and other studies (e.g. Fridlind et al., 2007; Morrison et al., 2008a). These other studies could maintain larger liquid amounts

with higher IN concentrations because spherical habits were used. We demonstrated that a large range of liquid and/or ice water path can be produced by reasonable changes in ice crystal habit mass-dimensional relations and the associated terminal fall-speed relations based on data reported in the literature. Our results also suggest that changes in ice crystal habit might be related to liquid layer formation, the splitting of liquid layers, and cloud dissipation mechanisms in multi-layered Arctic mixed-phase clouds. Furthermore, precisely because of the demonstrated sensitivity of model results to the choice of ice crystal habit, we conclude that simulating changes in crystal habit is of vital importance for correct model representation of mixed-phase clouds and a new approach, similar to Chen and Lamb's (1994) "adaptive growth" concept but applicable to Eulerian frameworks, is needed.

A problem common to all modeling studies of heterogeneous ice formation in mixed-phase clouds is the failure to reproduce observed ice crystal concentrations. This problem stems from the fact that measured IN concentrations (and consequently ice formation in models) are often several orders of magnitude lower than measured ice crystal concentrations. This discrepancy has not been resolved to date, though a number of possible nucleation mechanisms have been suggested.

Using a two-dimensional eddy-resolving model we examined three ice nucleation mechanisms ("evaporation IN", "evaporation freezing", and immersion freezing) with regard to their ability to: (1) correctly simulate liquid and ice water content and ice concentrations in Arctic mixed-phase clouds, and (2) correctly

reproduce the observed cloud structure. All of them were capable of producing ice crystal concentrations that are similar to the observed values, while maintaining the liquid water content of the cloud. Simulated liquid and ice water paths were also shown to match the observations. All three nucleation mechanisms could reproduce the observed cloud structure for extended periods of time. Preliminary analysis shows that identifying the location of ice formation may assist in distinguishing between these mechanisms. Immersion freezing produces ice at cloud top, deposition/condensation freezing produces ice everywhere, whereas “evaporation freezing” and “evaporation IN” tend to initiate ice in the downdrafts. Analysis of “evaporation IN” mechanism is complicated by the fact that it has both local and non-local effects. Ice can be formed locally at the same instant that the IN are formed, however the produced IN can also be advected. These IN can cause ice formation at a later time elsewhere in the cloud.

Bibliography

Avramov A. and J.Y. Harrington, 2006: The influence of ice nucleation mode and ice vapor growth on simulation of Arctic mixed-phase clouds. *12th Conference on Cloud Physics,* Madison, WI

Bigg, E. K. 1953: The supercooling of water, *Proc. Phys. Doc. London*, Sect. **B**, **66**, 688– 694.

Bigg, E. K., 1996: Ice forming nuclei in the high Arctic. *Tellus*, **48,** 223-233.

Cantrell, W., A. J. Heymsfield, 2005: Production of ice in tropospheric clouds: A review. *Bull. Amer. Meteor. Soc.*, **86**, 795-807

Carrió, G.G., H. Jiang, and W.R. Cotton, 2005: Impact of Aerosol Intrusions on Arctic Boundary Layer Clouds. Part I: 4 May 1998 Case. *J. Atmos. Sci.*, **62**, 3082–3093.

Chen, J.P., and D. Lamb, 1994: The Theoretical Basis for the Parameterization of Ice Crystal Habits: Growth by Vapor Deposition. *J. Atmos. Sci.*, **51**, 1206–1222.

Cotton, R. J., and P. R. Field 2002: Ice nucleation characteristics of an isolated wave cloud, *Quart. J. Roy. Meteor. Soc.*., **128**, 2417– 2437.

Cotton, W. R., G.J. Tripoli, R.M. Rauber, and E.A. Mulvihill, 1986: Numerical simulation of the effects of varying ice crystal nucleation rates and aggregation processes on orographic snowfall. *J. Clim. Apll. Meteorol.*, **25**, 1658-1680.

Cotton, W.R., M.A. Stephens, T. Nehrkorn and G.J. Tripoli, 1982: The Colorado State University three-dimensional cloud/mesoscale model - 1982. Part II: An ice phase parameterization. *J. de Rech. Atmos.,* **16**, 295-320.

Cotton, W. R., R.A. Pielke, Sr., R.L. Walko , G.E. Liston, C.J. Tremback, H. Jiang, R. L. McAnelly, J.Y. Harrington, M.E. Nicholls, G.G. Carrió and J. P. Mc Fadden 2003: RAMS 2001: Current Status and future directions. *Meteor. Atmos. Physics* **82**, 5-29.

Curry, J., W. Rossow, D. Randall, and J. Schramm, 1996: Overview of arctic cloud and radiation characteristics. *J. Climate*, **9**, 1731-1764.

Curry, J. A. and A. H. Lynch, 2002: Comparing Arctic regional climate models. *EOS*, **83,** 87.

DeMott, P.J, M.P. Meyers, and W.R. Cotton, 1994: Parameterization and impact of ice initiation processes relevant to numerical model simulations of cirrus clouds. *J. Atmos. Sci.*, **51**, 77-90.

Fridlind, A.M., A.S. Ackerman, G. McFarquhar, G. Zhang, M.R. Poellot, P.J. DeMott, A.J. Prenni, and A.J. Heymsfield, 2007: Ice properties of single-layer stratocumulus during the Mixed-Phase Arctic Cloud Experiment (M-PACE): Part II, Model results. *J. Geophys. Res.*, **112**, D24202, doi:10.1029/2007JD008646.

Harrington, J.Y., M.P. Meyers, R.L. Walko, and W.R. Cotton, 1995: Parameterization of ice crystal conversion processes due to vapor deposition for mesoscale models using double-moment basis functions. Part I: Basic formulation and parcel model test. *J. Atmos. Sci.*, **52**, 4344-4366.

Harrington, J. Y., T. Reisin, W. R. Cotton, and S. M. Kreidenweis, 1999: Cloud resolving simu-lations of Arctic stratus. Part II: Transition-season clouds. *Atmos. Res.,* **51,** 45–75.

Harrington, J. Y. and P. Q. Olsson, 2001a: On the potential influence of ice nuclei on surface-forced marine stratocumulus cloud dynamics. *J. Geophys. Res.,* **106**, 27473-27484.

Harrington, J. Y. and P. Q. Olsson, 2001b: A method for the parameterization of cloud radiative properties within numerical models. Atmos. Res., **57**, 51-80.

Heymsfield, A. J., and Kajikawa, M., 1987: An improved approach to calculating terminal velocities of plate-like crystals and graupel. *J. Atmos. Sci*., **44**, 1088-1099.

Heymsfield, A. J., , A. Bansemer, S. Lewis, J. Iaquinta, M. Kajikawa, C. Twohy, M. R. Poellot, and L. M. Miloshevich, 2002: A general approach for deriving the properties of cirrus and stratiform ice cloud particles. J*. Atmos. Sci.,* **59**, 3-29.

Hobbs P. V., and A. L. Rangno, 1998: Microstructure of low- and middle-level clouds over the Beaufort Sea. *Quart. J. Roy. Meteor. Soc.*, **124**, 2035–2071.

Houghton, J. T., G. J. Jenkins, and J. J. Ephraums (Eds.), 1990: Climate Change. The IPCC Scientific Assessment, World Meteorological Organization/United Nations Environment Programme. Cambridge University Press.

Jiang, H., W.R. Cotton, J.O. Pinto, J.A. Curry, and M.J. Weissbluth, 2000: Sensitivity of mixedphase Arctic stratocumulus to ice forming nuclei and large-scale heat and moisture advection. *J. Atmos. Sci.*, **57**, 2105-2117.

Klein, S., R. McCoy, H. Morrison, A. Ackerman, A. Avramov, G. deBoer, M. Chen, J. Cole, A. DelGenio, M. Falk, M. Foster, A. Fridlind, J. C. Golaz, T. Hashino, J. Harrington, C. Hoose, M. Khairoutdinov, V. Larson, X. Liu, Y. Luo, G. McFarquhar, S. Menon, R. Neggers, S. Park, M. Poellot, K. Salzen, J. Schmidt, I. Sednev, B. Shipway, M. Shupe, D. Spangenberg, Y. Sud, D. Turner, D Veron, G. Walker, Z. Wang, A. Wolf, S. Xie, K.-M. Xu, F. Yang, and G. Zhang, 2008: Intercomparison of model simulations of mixed-phase clouds observed during the ARM Mixed-Phase Arctic Cloud Experiment. Part I: Single layer cloud. *submitted to Quart. J. Roy. Meteor. Soc.*

Korolev, A., 2007: Limitations of the Wegener–Bergeron–Findeisen Mechanism in the Evolution of Mixed-Phase Clouds. *J. Atmos. Sci.*, **64**, 3372–3375.

Korolev A. V., and G. A. Isaac, 2003: Phase transformation in mixed-phase clouds. *Quart. J. Roy. Meteor. Soc.*, **129**, 19–38.

Korolev, A., and P.R. Field, 2008: The Effect of Dynamics on Mixed-Phase Clouds: Theoretical Considerations. *J. Atmos. Sci.*, **65**, 66–86.

McFarquhar G. M., G. Zhang, M. R. Poellot, G. L. Kok, R. McCoy, T. Tooman, A. Fridlind, and A. J. Heymsfield, 2007: Ice properties of single-layer stratocumulus during the Mixed-Phase Arctic Cloud Experiment. 1. Observations. *J. Geophys. Res.*, **112**, D24201, doi:10.1029/2007JD008633.

Meyers, M.P., P.J. Demott, and W.R. Cotton, 1992: New primary ice-nucleation parameterizations in an explicit cloud model. *J. Appl. Meteor*, **31**, 708-721.

Meyers, M.P., R.L. Walko, J.Y. Harrington, and W.R. Cotton, 1997: New RAMS cloud microphysics parameterization. 2. The two-moment scheme. *Atmos. Res.*, **45**, 3, 39.

Mitchell, D.L., 1996: Use of Mass- and Area-Dimensional Power Laws for Determining Precipitation Particle Terminal Velocities. *J. Atmos. Sci.*, **53**, 1710–1723.

Morrison, H., and J. O. Pinto, 2005: Mesoscale modeling of springtime arctic mixed-phase stratiform clouds using a new two-moment bulk microphysics scheme, *J.Atmos. Sci., **62***, 3683-3704.

Morrison, H., M.D. Shupe, J.O. Pinto, and J.A. Curry, 2005: Possible roles of ice nucleation mode and ice nuclei depletion in the extended lifetime of Arctic mixed-phase clouds. *Geophys Res. Lett,* **32**, doi:10.1029/2005GL023614.

Morrison, H., J. O. Pinto, J. A. Curry, and G. M. McFarquhar, 2008a: Sensitivity of modeled arctic mixed-phase stratocumulus to cloud condensation and ice nuclei over regionally varying surface conditions, *J. Geophys. Res.*, **113**, D05203, doi:10.1029/2007JD008729.

Morrison H., R. McCoy, S. Klein, S. Xie, Y. Luo, A. Avramov, M. Chen, J. Cole, M. Falk , M. Foster, A. DelGenio, J. Harrington, C. Hoose , M. Khrairoutdinov, V. Larson, X. Liu, G. McFarquhar1, M. Poellot, K. Salzen, B. Shipway, M. Shupe, Y. Sud, D. Turner, D. Veron, G. Walker, Z. Wang, A. Wolf, K.–M. Xu, F. Yang,and G. Zhan, 2008: Intercomparison of model simulations of mixed-phase clouds observed during the ARM Mixed-Phase Arctic Cloud Experiment, Part II: Multi-layered cloud. *submitted to Quart. J. Roy. Meteor. Soc.*

Mossop, S., 1970: Concentrations of Ice Crystals in Clouds. *Bull. Amer. Meteor. Soc.*, **51**, 474–479.

Mossop, S., 1985: The Origin and Concentration of Ice Crystals in Clouds. *Bull. Amer. Meteor. Soc.*, **66**, 264–273.

Pinto, J.O., 1998: Autumnal mixed-phase cloudy boundary layers in the Arctic. *J. Atmos. Sci.*, **55**, 2016-2038.

Prenni, A.J., J.Y. Harrington, M. Tjernstrom, P.J. DeMott, A. Avramov, C.N. Long, S.M. Kreidenweis, P.Q. Olsson, and J. Verlinde, 2006: Can ice-nucleating aerosols affect Arctic seasonal climate? *Bull. Am. Meteorol. Soc.*, **88,** 541-550.

Pruppacher, H. R. and Klett, J. D. 1997 *Microphysics of clouds and precipitation.* 2nd edition, Kluwer Academic Publishers, Dordrecht, The Netherlands.

Rauber, R., and A. Tokay, 1991: An explanation for the existence of supercooled water at the top of cold clouds. *J. Atmos. Sci*., **48**, 1005-1023.

Reisin, T., Z. Levin, and S. Tzivion, 1996: Rain Production in Convective Clouds As Simulated in an Axisymmetric Model with Detailed Microphysics. Part I: Description of the Model. *J. Atmos. Sci.*, **53**, 497–519.

Rogers, D.C., P.J. DeMott, and S.M. Kreidenweis, 2001: Airborne measurements of tropospheric ice-nucleating aerosol particles in the Arctic spring. *J. Geophys. Res.*, **106**, 15053-15063.

Rosinski, J., and G. Morgan 1991: Cloud condensation nuclei as a source of ice-forming nuclei in clouds. *J. Aerosol Sci.*, **22**, 123–133.

Seroka, G.N., 2008: Arctic Mixed-Phase Cloud Microphysics and Dynamics From Doppler Radar Spectra. *BSc thesis*. The Pennsylvania State University.

Sheridan, L.M., J.Y. Harrington and D. Lamb, 2008: Ice Crystal Habit Influence on Size Spectra Evolution during Vapor Depositional Growth. *to be submitted*

Shupe, M.D., and J.M. Intrieri, 2004: Cloud radiative forcing of the Arctic surface: The influence of cloud properties, surface albedo, and solar zenith angle. *J. Climate*, **17**, 616-628.

Shupe, M.D., S.Y. Matrosov, and T. Uttal, 2006: Arctic mixed-phase cloud properties derive from surface-based sensors at SHEBA. *J. Atmos. Sci.*, **63**, 697-711.

Tao, X., J. E. Walsh and W. L. Chapman, 1996: An assesment of global climate model simulations of arctic air temperatures, *J. Climate*, **9**, 1060-1076.

Turner, D.D., S.A. Clough, J.C. Liljegren, E.E. Clothiaux, K. Cady-Pereira, and K.L. Gaustad, 2007: Retrieving liquid water path and precipitable water vapor from Atmospheric Radiation Measurement (ARM) microwave radiometers. *IEEE Trans. Geosci. Remote Sens.*, **45**, 3680-3690

Uttal, T., J.A. Curry, M.G. Mcphee, D.K. Perovich, R.E. Moritz, J.A. Maslanik, P.S. Guest, H.L. Stern, J.A. Moore, R. Turenne, A. Heiberg, M.C. Serreze, D.P. Wylie, O.G. Persson, C.A. Paulson, C. Halle, J.H. Morison, P.A. Wheeler, A. Makshtas, H. Welch, M.D. Shupe, J.M. Intrieri, K. Stamnes, R.W. Lindsey, R. Pinkel, W.S. Pegau, T.P. Stanton, and T.C. Grenfeld, 2002: Surface Heat Budget of the Arctic Ocean. *Bull. Amer. Meteor. Soc.*, **83**, 255–275.

Vavrus, S., 2004: The impact of cloud feedbacks on arctic climate under greenhouse forcing. *J. Climate*, **17**, 603-615.

Verlinde, J., J. Y. Harrington, G. M. McFarquhar, V.T. Yanuzzi, A. Avramov, S. Greenberg, N. Johnson, M. R. Poellot, J. H. Mather, D. D. Turner, B. D. Zak, T. Tooman, A. J. Prenni, G. L. Kok, E. W. Eloranta, M. D. Ivey, C. P. Bahrmann, K. Sassen, P. J. DeMott, A. J. Heymsfield, 2006: The mixed-

phase Arctic cloud experiment (M-PACE). *Bull. Am. Meteorol. Soc.,* **88,** 205-221.

Walko, R.L., W.R. Cotton, M.P. Meyers, and J.Y. Harrington, 1995: New RAMS cloud micro-physics parametrization. 1. The single-moment scheme. *Atmos. Res*., **38**, 29-62.

Walsh, J. E. and R. G. Crane., 1992: A comparison of GCM simulations of Arctic climate. *Geophys. Res. Lett.*, **19**, 29-32.

Westbrook, C.D., R.J. Hogan, and A.J. Illingworth, 2008: The Capacitance of Pristine Ice Crystals and Aggregate Snowflakes. *J. Atmos. Sci.*, **65**, 206–219.

Yannuzzi, V. T., 2007: A Statistical Comparison of Forecasting Models Across the North Slope of Alaska During the Mixed-Phase Arctic Cloud Experiment. *MSc thesis*. The Pennsylvania State University.

Young, K.C., 1974: The Role of Contact Nucleation in Ice Phase Initiation in Clouds. *J. Atmos. Sci.*, **31**, 768–776.

Zuidema, P., B. Baker, Y. Han, J. Intrieri, J. Key, P. Lawson, S. Matrosov, M. Shupe, R. Stone, and T. Uttal, 2005: An Arctic Springtime Mixed-Phase Cloudy Boundary Layer Observed during SHEBA. *J. Atmos. Sci.*, **62**, 160–176.

VITA

EDUCATION

Ph. D.	Meteorology	The Pennsylvania State University	May 2009
M. S.	Meteorology	The Pennsylvania State University	December 2005
M. S.	Physics	Sofia University	October 1993

EMPLOYMENT

Aug. 2001 – Dec. 2008, Research Assistant, Dept. of Meteorology, Penn State University
Aug. 2000 – Aug. 2001, System Administrator, Zeitungsgruppe Bulgarien, Sofia, Bulgaria
Oct. 1993 – Aug. 2000, Physicist, Head of R&D Division, Hail Suppression Agency, Bulgaria

REFEREED PUBLICATIONS:

Donev E., Zeller K., Avramov A., 1998: Influence of valley winds on summertime ozone concentration at sloped Bulgarian mountain site. *Journal of Balkan Ecology*, vol.1, No 4

Donev E., Ivanova D., Avramov A., Zeller K., 1999: Rank correlation approach to assessing influence of mountain valley winds on ozone concentration. *Journal of Balkan Ecology,* vol.2, No 2

Avramov A., Donev E., Zeller K.,1999: A composite Regression Model of the Ozone Dependence on Meteorology in Mountain Valley site. *Bulgarian Journal of Meteorology and Hydrology*, vol.10, No 3 - 4, pp. 67 – 75

Donev E., Zeller, K. and A. Avramov, 2002: Preliminary background ozone concentrations in the mountain and coastal areas of Bulgaria. *Environmental Pollution*, **17**, 281-286.

Verlinde J., J.Y. Harrington, G.M. McFarquhar, V.T. Yannuzzi, A. Avramov, S. Greenberg, N. Johnson, G. Zhang, M.R. Poellot, J.H. Mather, D.D. Turner, E.W. Eloranta, B.D. Zak, A.J. Prenni, J.S. Daniel, G.L. Kok, D.C. Tobin, R. Holz, K. Sassen, D. Spangen, 2007: The Mixed-Phase Arctic Cloud Experiment (M-PACE). *Bull. Amer. Meteor. Soc*, 88, 205-221.

Prenni A.J., J.Y. Harrington, M. Tjernstrom, P. J. DeMott, A. Avramov, C. N. Long, S.M. Kreidenweis, P.Q. Olsson, J. Verlinde, 2007: Can Ice-Nucleating Aerosols Affect Arctic Seasonal Climate?. *Bull. Amer. Meteor. Soc*, 88, 541-550.

Klein et al., 2008: Intercomparison of model simulations of mixed-phase clouds observed during the ARM Mixed-Phase Arctic Cloud Experiment. Part I: Single layer cloud. Submitted to *Q. J. Roy. Meteor. Soc*.

Morrison et al. 2008: Intercomparison of model simulations of mixed-phase clouds observed during the ARM Mixed-Phase Arctic Cloud Experiment, Part II: Multilayered Cloud. Submitted to *Q. J. Roy. Meteor. Soc*.

Avramov A. and J.Y. Harrington, 2009: On the potential influence of parameterized ice crystal habit on simulations of Arctic mixed-phase clouds *(to be submitted to Journal of Geophysical Research)*

Avramov, A., J. Harrington, and J. Verlinde, 2009: On the possible influence of ice nucleating mechanisms on simulated mixed-phase cloud structure: Comparison to radar observations. *(to be submitted to Journal of the Atmospheric Sciences)*